© 2022. Published by The Company of Biologists Ltd | Journal of Cell Science (2022) 135, jcs259893. doi:10.1242/jcs.259893

RESEARCH ARTICLE

TFK1, a basal body transition fibre protein that is essential for cytokinesis in *Trypanosoma brucei*

Miharisoa Rijatiana Ramanantsalama[1], Nicolas Landrein[1], Elina Casas[1], Bénédicte Salin[2], Corinne Blancard[2], Mélanie Bonhivers[1], Derrick R. Robinson[1] and Denis Dacheux[1,3,*]

ABSTRACT

In *Trypanosoma brucei*, transition fibres (TFs) form a nine-bladed pattern-like structure connecting the base of the flagellum to the flagellar pocket membrane. Despite the characterization of two TF proteins, CEP164C and *T. brucei* (Tb)RP2, little is known about the organization of these fibres. Here, we report the identification and characterization of the first kinetoplastid-specific TF protein, named TFK1 (Tb927.6.1180). Bioinformatics and functional domain analysis identified three distinct domains in TFK1 – an N-terminal domain of an unpredicted function, a coiled-coil domain involved in TFK1–TFK1 interaction and a C-terminal intrinsically disordered region potentially involved in protein interaction. Cellular immunolocalization showed that TFK1 is a newly identified basal body maturation marker. Furthermore, using ultrastructure expansion and immuno-electron microscopies we localized CEP164C and TbRP2 at the TF, and TFK1 on the distal appendage matrix of the TF. Importantly, RNAi-mediated knockdown of TFK1 in bloodstream form cells induced misplacement of basal bodies, a defect in the furrow or fold generation, and eventually cell death. We hypothesize that TFK1 is a basal body positioning-specific actor and a key regulator of cytokinesis in the bloodstream form *Trypanosoma brucei*.

KEY WORDS: *Trypanosoma brucei*, Transition fibre, Transition fibre protein kinetoplastid specific-1, TFK1, Cytokinesis, Basal body, Flagellum, Kinetoplastid, Cytoskeleton

INTRODUCTION

Trypanosoma brucei is a unicellular flagellated African protozoan parasite responsible for human African trypanosomiasis or 'sleeping sickness', and nagana in livestock (Auty et al., 2015; Büscher et al., 2017; Steverding, 2008). *T. brucei* has complex life and cell cycles during transmission from the tsetse fly vector to the mammalian host with significant morphogenetic changes (Gull, 1999; Matthews, 1999). Among the different forms are the procyclic insect form (PCF) in the insect midgut and the infectious bloodstream form (BSF), found upon transmission to the vertebrate host.

In both forms, a single flagellum nucleates from the basal body (BB) near the posterior end of the cell, exits the cell body through the flagellar pocket (FP), the only site for endocytosis and exocytosis, and extends along the length of the cell toward the anterior end (Field and Carrington, 2009; Lacomble et al., 2009, 2010; Overath and Engstler, 2004). The cytoskeleton region between the BBs and the site where the flagellum exits the cell is quite complex. The BBs are connected to the mitochondrial genome (kinetoplast) through the tripartite attachment complex (TAC) but also with the FP membrane through the transition fibres (TFs) (Ogbadoyi et al., 2003; Vaughan and Gull, 2016). The TFs consist of a set of nine structures that are located on the mature BB and radiate from the triplet of microtubules to connect it to the FP membrane (Geimer and Melkonian, 2004; Gonçalves and Pelletier, 2017; Lacomble et al., 2009; O'Toole et al., 2003; Trépout et al., 2018; Vaughan and Gull, 2016). The flagellum remains attached to the cell body via a junctional complex known as the flagellar attachment zone (FAZ) (Sunter and Gull, 2016). A set of four specialized microtubules (the microtubule quartet; MtQ) nucleates between the mature (BB) and the pro-basal bodies (pBB), wraps around the FP and continues along the flagellar pocket collar (FPC) to extend up to the anterior end of the cell body (Gheiratmand et al., 2013; Robinson et al., 1995; Taylor and Godfrey, 1969).

PCFs and BSFs divide slightly differently but share the same cytokinesis stages, characterized by the duplication of the single-copy organelles and their segregation leading to two daughter cells (schematized in Fig. S1a and b, respectively) (Vickerman, 1962; Sinclair and de Graffenried, 2019; Wheeler et al., 2013; Sherwin et al., 1989; Robinson et al., 1995; Farr and Gull, 2012). Those events are associated chronologically with pro-BB maturation, new flagellum growth, BB segregation, and finally, cytokinesis combined with abscission (Fig. S1) (Wheeler et al., 2013, 2019). In *T. brucei*, the first noticeable events of the cell cycle are BB maturation, the nucleation of a new MtQ and the biogenesis of a new flagellum (Lacomble et al., 2009, 2010). Tight regulation of these events is critical for the parasite for ensuring the correct position of the fold that determines the shape and form of the daughter cells and thereafter furrow ingression (Lacomble et al., 2010). The evolutionarily conserved protein kinases Aurora B kinase 1 [*T. brucei* (Tb)AUK1] and Polo-like kinase (TbPLK) might be involved in BB segregation (Ikeda and de Graffenried, 2012), whereas TbNRKC (NIMA related kinase C) is involved in replication and segregation and TbLRTP is involved in their replication (Morgan et al., 2005; Pradel et al., 2006). TbPLK has been shown to interact with numerous trypanosome-specific proteins including the cytokinesis regulator TOEFAZ1 (also known as CIF1) protein (McAllaster et al., 2015; Zhou et al., 2016a). TOEFAZ1 accumulates at the new FAZ tip in a complex with the CIF2 and CIF3 proteins, all involved in cytokinesis furrow initiation (Zhou et al., 2016a; Kurasawa et al., 2018, 2022). In contrast to most higher eukaryotes, which rely on a contractile actomyosin ring, abscission in *T. brucei* requires flagellar

[1]University of Bordeaux, CNRS, Microbiologie Fondamentale et Pathogénicité, UMR 5234, F-33000 Bordeaux, France. [2]University of Bordeaux, CNRS, Microscopy Department IBGC, UMR 5095, F-33000 Bordeaux, France. [3]Bordeaux INP, Microbiologie Fondamentale et Pathogénicité, UMR 5234, F-33000 Bordeaux, France.

*Author for correspondence (ddacheux@bordeaux-inp.fr)

M.R.R., 0000-0003-3530-9756; N.L., 0000-0001-8875-4242; E.C., 0000-0001-5783-7459; B.S., 0000-0003-2423-6360; C.B., 0000-0002-3335-0942; M.B., 0000-0001-9179-8473; D.R.R., 0000-0001-5572-4127; D.D., 0000-0002-9956-4839

Handling Editor: David Stephens
Received 7 February 2022; Accepted 12 May 2022

Journal of Cell Science (2022) 135, jcs259893. doi:10.1242/jcs.259893

movements (Broadhead et al., 2006; Ralston et al., 2006) or an undiscovered membrane fission mechanism (Farr and Gull, 2012).

In eukaryotic cells, centrioles are structures with a diameter of ∼250 nm and with a length ranging between 150 nm and 500 nm (Winey and O'Toole, 2014). In a pair of centrioles, only the mother centriole (MC; i.e. the mature centriole) bears distal appendages distal appendages (DAs) and sub-distal appendages (SDAs) (Hatch and Stearns, 2010). The DAs are shaped as radial nine-fold twisted arrangement structures with fibres located centrally and symmetrically at the distal end of the mother centriole. Each DA is associated with one of the centriole triplets with an angle of ∼50° (Uzbekov and Alieva, 2018). SDAs are conical-shaped structures linked to the centrosomal barrel by two axonemal microtubules triplets (Paintrand et al., 1992; Uzbekov and Alieva, 2018; Winey and O'Toole, 2014). These appendages (DA and SDA) are required for ciliogenesis and MC transformation into a BB (Hall and Hehnly, 2021; Jana et al., 2014; Paintrand et al., 1992). MCs and BBs are similar in structure and function, and the TFs that correspond to the DAs of the MC extend from the BB and connect to the plasma membrane to initiate ciliogenesis (Hall and Hehnly, 2021; Kobayashi and Dynlacht, 2011; Kumar and Reiter, 2021; Paintrand et al., 1992; Pearson, 2014). The TFs provide a physical demarcation of the flagellum/cilium compartment from the rest of the cell, allowing the recruitment and selective transport of proteins by the IFT machinery, which is essential for axoneme elongation and maintenance (Reiter et al., 2012; Wei et al., 2015). TF and DA components are well preserved among ciliated organisms, including CEP83, CEP89 and CEP164 (centrosomal proteins), sodium channel and clathrin linker 1 (SCLT1), ankyrin repeat domain containing 26 (ANKRD26), which forms the backbone of blades, and Fas-binding factor 1 (FBF1), which localizes within the distal appendage matrix (DAM) between the appendage blades in proximity to the ciliary membrane (Bowler et al., 2019; Chong et al., 2020; Graser et al., 2007; Greenan et al., 2020; Hodges et al., 2010; Joo et al., 2013; Tanos et al., 2013; Tischer et al., 2021; Wei et al., 2013; Yang et al., 2018). Recently, a bioinformatics analysis has identified orthologs of CEP164 and ANKRD26 in *T. brucei* (Tischer et al., 2021).

The trypanosome mature BB is composed of nine microtubule triplets followed by the TFs (Vaughan and Gull, 2016) and the transition zone (TZ) (Lacomble et al., 2009; Trépout et al., 2018; Vaughan and Gull, 2016). Together, the TFs and TZ constitute the ciliary gate, which serves as docking sites and regulators for intraflagellar transport and is involved in forming functional ciliary compartments in cilia and flagella (Reiter et al., 2012; Dean et al., 2016). To date, only two proteins have been identified as TF proteins in *T. brucei*, TbRP2 and CEP164C (Atkins et al., 2021; Stephan et al., 2007). In eukaryotes, RP2 and CEP164 proteins are conserved and embedded at the TFs of the mature BB where they provide an essential cilium/flagellum-specific function (Andre et al., 2014; Gonçalves and Pelletier, 2017; Graser et al., 2007; Reiter et al., 2012; Slaats et al., 2014; Stephan et al., 2007). In dividing trypanosome cells, TbRP2 is observed at the TF in both the old and the new flagella (Andre et al., 2014; Stephan et al., 2007), whereas CEP164C is present only on the TF of the old flagellum (Atkins et al., 2021). RNA interference (RNAi)-mediated knockdown of TbRP2 leads to an axonemal microtubule formation defect, disturbs the recruitment of TZ proteins and induces loss of tyrosinated α-tubulin on the mature BB without affecting the other microtubules (Stephan et al., 2007; Harmer et al., 2017; Atkins et al., 2021). The depletion of CEP164C induces dysregulation of the old flagellum growth due to a defect in the locking mechanism that regulates old and new flagella growth (Atkins et al., 2021).

Here, we have identified and characterized the protein transition fibre kinetoplastid-specific protein 1 (TFK1; Tb927.6.1180) as the first matrix TF protein in *T. brucei* that is specific to kinetoplastids. Our high-resolution ultrastructure expansion microscopy (U-ExM) data demonstrate new insight into the TF organization in *T. brucei* with distinct localization of TbRP2, CEP164C and TFK1. Our data reveal that TKF1 is composed of several predicted coiled-coil domains and an intrinsically disordered region (IDR). RNAi-mediated knockdown of TFK1 in BSF induces previously undescribed cytokinesis defects that are ultimately lethal. Our results suggest an essential role for TFK1 in the coordination of certain cytoskeleton components during cell division of BSF *T. brucei*.

RESULTS

TFK1 is a kinetoplastid-specific coiled-coil protein

Tb927.6.1180 protein (ProteinID: XP_845240.1) was first identified as a potential BILBO1-binding partner, with a low interaction reliability predicted biological score, in a *T. brucei* 927 genomic yeast two-hybrid screen (Hybrigenics) using BILBO1 as bait (Albisetti et al., 2017). Here, we identified Tb927.6.1180 as a novel BB protein and designated it as TFK1 for transition fibre kinetoplastid-specific protein 1. TFK1 is a 141.19 kDa protein consisting of 1271 amino acids with a calculated pI of 5.25 encoded by a single-copy gene located on chromosome 6 (Fig. 1A). TFK1 primary structure is composed of three distinct regions: (1) an N-terminal region [amino acids (aa) 1–74] with no predicted function, (2) a large central region (aa 75–802) consisting of two coiled-coil regions CC1 (aa 75–536) and CC2 (aa 537–802), and (3) a C-terminal region (aa 803–1271) predicted as an intrinsically disordered region (IDR) (Fig. 1A). Furthermore, the presence of the coiled-coil and IDR domains suggests that TFK1 could form a homodimer and interact with other protein partners (Barbar and Nyarko, 2015; Kuhn et al., 2014; Uversky, 2013). Orthologs searches using BLAST-P, PSI-BLAST and HMMER (Altschul, 1997; Altschul et al., 2005; Finn et al., 2011) identified orthologs but only in the Kinetoplastea class with a conserved gene synteny. The TFK1 orthologs have an estimated molecular mass ranging from 118.41 to 160.11 kDa (for *Phytomonas* sp. and *T. vivax*, respectively). A multiple sequence alignment using ClustalOmega identified the three conserved main regions (the N-terminal domain, coiled-coil domain and IDR) among the TFK1 orthologs (Fig. S2) (Madeira et al., 2019).

TFK1 is located on the mature BB

To assess the localization of TFK1, we generated a mouse monoclonal antibody (anti-TFK1 antibody) against the full-length purified TFK1 protein (Fig. S3A,B). Immunoblots of *T. brucei* cell lysates showed that anti-TFK1 recognized the wild-type (WT) TFK1 protein (141.19 kDa) in PCF and BSF forms (Fig. 1B) as well as an endogenously N-terminally TY1-tagged version of TFK1 (152.9 kDa) generated following the protocol described in Dean et al. (2015) (Fig. S3C,D). The anti-TFK1 labelling revealed a major band at the expected size but also several other bands in both PCF and BSF cells (Fig. 1B). These bands diminished after TFK1 RNAi knockdown experiments (described below) (Fig. S3C,D) and could reflect the phosphorylation status of the serine residues S898, S906, S1104 and S919 identified in phosphoproteomic analyses (Nett et al., 2009; Urbaniak et al., 2013), or be due to proteolysis during cell lysis due to the presence of potential cleavage sites in the

Journal of Cell Science

Journal of Cell Science (2022) 135, jcs259893. doi:10.1242/jcs.259893

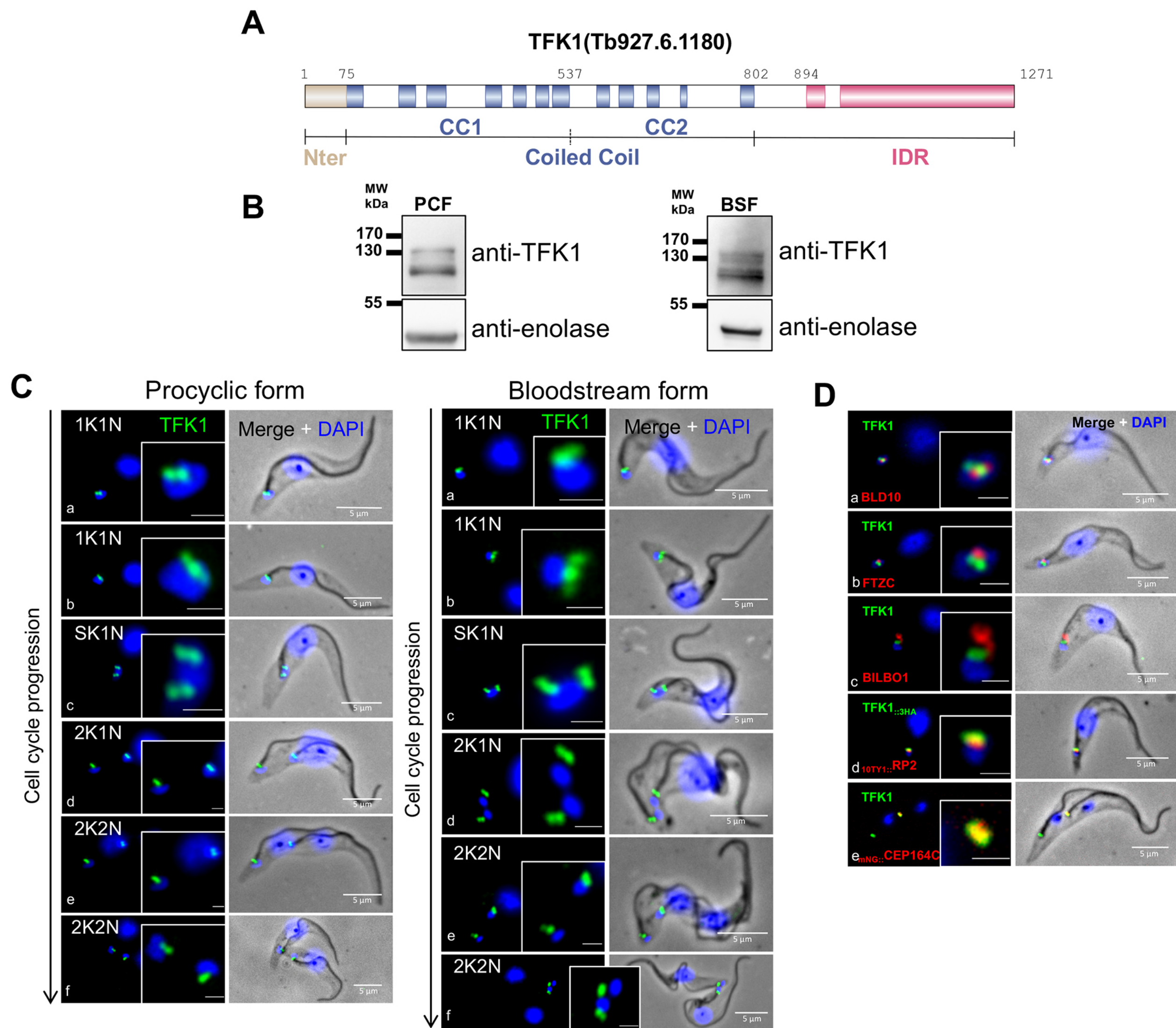

Fig. 1. TFK1 is a coiled-coil protein localized at the BB region. (A) Representation of TFK1 (Tb927.6.1180) domains: an N-terminal region (aa 1–74), a central coiled-coil region (aa 75-802) composed of 12 coiled-coil protein domains divided into CC1 (aa 75–536) and CC2 (aa 537–802), and a C-terminal intrinsically disordered region (IDR) (aa 803–1271). (B) Western blots of TFK1 using anti-TFK1 in PCF and BSF wild-type whole cells (enolase as loading charge). (C) Immunofluorescence labelling on detergent-extracted cells for TFK1 (green, anti-TFK1) across the cell cycle in PCF and BSF forms. (D) Immunofluorescence on detergent-extracted cells showing the colocalization of TFK1 (green, anti-TFK1) with BLD10 (red, a BB marker) (a), FTZC (red, a TZ marker) (b), BILBO1 (red, flagellar pocket collar marker) (c), endogenously tagged TY1::RP2 (red) (d) and mNeonGreen::CEP164C (red) (e). Scale bars: 5 µm (main images), 1 µm (insets). Images shown are representative of three experiments.

C-terminal domain of TFK1. As previously observed on the TrypTag genome-wide protein localization resource (http://tryptag.org/), which localized an endogenously N-terminally mNeonGreen-tagged form of TFK 1 in the BB area (Dean et al., 2016), our anti-TFK1 antibody labelling was observed as two dots close to the kinetoplast in whole cells but also in detergent-extracted cytoskeletons of PCF and BSF cells (Fig. S3E and Fig. 1Ca, respectively). This labelling colocalized with an anti-HA tag labelling of endogenously tagged TFK1::HA (Fig. S3E). The presence of a N-terminal or C-terminal tag did not affect the TFK1 localization (Fig. S3E). Importantly, this labelling was also maintained on detergent-extracted cytoskeletons of PCF and BSF cells, indicating that the TFK1 protein is a cytoskeleton-associated protein localizing on or close to the BBs (Fig. 1Ca).

Further analysis of the immunolabelling using the anti-TFK1 antibody showed that TFK1 is present throughout the cell cycle at the base of both the old and the new flagellum in PCF and BSF cells (Fig. 1C). We thus wanted to colabel TFK1 with the BBs and flagellum-associated cytoskeleton protein markers BLD10, FTZC, CEP164C, TbRP2 and BILBO1. BLD10 is a conserved cartwheel protein (Carvalho-Santos et al., 2010) that stabilizes the nine-fold symmetry of the centriole in *Chlamydomonas* (Hiraki et al., 2007; Matsuura et al., 2004) and controls the formation of the flagellum central pair in *Drosophila* spermatozoid (Carvalho-Santos et al., 2012). BLD10 was also identified by bioinformatics and proximity-dependent biotin identification as a *T. brucei* BB component (Dang et al., 2017). BLD10 localizes at both the mature and the immature BB throughout the cell cycle (Dang et al., 2017; Geimer and Melkonian, 2004). FTZC (for flagellar transition zone component) is a *T. brucei*-specific protein localized at the perimeter of the TZ and thus can be used to localize the mature BB (Bringaud et al., 2000; Gorilak et al., 2021). CEP164C is a TF protein that plays a

Journal of Cell Science

Journal of Cell Science (2022) 135, jcs259893. doi:10.1242/jcs.259893

role in the regulation of the *T. brucei* old flagellum length (Atkins et al., 2021) and TbRP2 is an α-tubulin binding and TFs protein involved in flagellum structure (Stephan et al., 2007) and in targeting of the ciliary gates TbMKS1 and TbMKS6 proteins (Andre et al., 2014). TbBILBO1 is one of the components of the FPC, a cytoskeleton structure distal to the transition zone that maintains the flagellar pocket enclosed around the flagellum (Bonhivers et al., 2008). BILBO1 is also present at the BB and most probably along the MtQ between the BBs and the FPC (Broster Reix et al., 2021a; Perdomo et al., 2022). To carry out these colabelling experiments we generated PCF cell lines expressing endogenously tagged N-terminal 10×TY1 tagged TFK1 (TY1::TFK1). To label the TFs, we generated a cell line expressing endogenously tagged TY1::TbRP2, and used a mNeonGreen (mNG)::CEP164C-expressing PCF cell line (Atkins et al., 2021). Immunofluorescence assays in both PCF and BSF using anti-BLD10 antibody (Dang et al., 2017) showed that despite signal being close to the BB, TFK1 does not colocalize with this BB marker (Fig. 1Da; Fig. S4Aa) and is proximal to the FTZC labelling and to the FPC marker (BILBO1) (Fig. 1Db,c and Fig. S4Ab,c respectively). Interestingly, TFK1 colocalized, at least partially, with the two TF proteins TbRP2 and CEP164C (Fig. 1Dd and De, respectively).

TFK1 is a TF protein

To analyse in more detail the BB localization of TFK1 by increasing the spatial resolution, we used U-ExM (Amodeo et al., 2021; Gambarotto et al., 2021). TFK1::HA was colabelled on detergent-extracted PCF cells with the cytoskeletal markers described above (Fig. 2). TFK1 appears as one set of nine individual dots organized in a circular fashion (Fig. 2Aa). This circular arrangement had average diameters of 1617 nm (inner) and 2533 nm (outer) which, after taking into account the expansion factor, indicates average diameters of 356 nm (inner) and 558 nm (outer) (n=10) (Fig. S4B). The BBs can be identified by BLD10 labelling, with BLD10 forming the cartwheel structure of the mature BB and the pro-BB (pBB) (Dang et al., 2017), whereas in G1 trypanosome cells, CEP164C labels the mature BB only (Atkins et al., 2021). At the early SK1N (early kinetoplast S phase) stage of the cell cycle, the BB and pro-BB or the maturing pro-BB (pBBm) are identified by BLD10 labelling (Dang et al., 2017). In these cells, TFK1 was only present on the mature BB (Fig. 2Aa,e), and at a slightly later stage was also on the maturing pro-BB (pBBm) as shown with the BLD10 colabelling (Fig. 2Ba,b). To distinguish between the BB and the maturing pro-BB, we used the mNG::CEP164C-expressing cell line (Atkins et al., 2021). In Fig. 2Ab, we show the first high-resolution localization of CEP164C, which adopted a punctuated radial arrangement, in agreement with the arrangement on TFs shown for the human ortholog CEP164 (Yang et al., 2018). Also, CEP164C labelling appeared unregular in intensity and positioning suggesting a localization on different planes (Fig. 2Ab), which is similar to the organization described for human ortholog CEP164 forming the backbone of the nine DA blades (Yang et al., 2018). Interestingly, the colabelling of TFK1 with CEP164C demonstrates that TFK1 is associated with the CEP164C-positive mature BB labelling suggesting that TFK1 is a mature BB or maturing pro-BB protein (Fig. 2Ab). Interestingly, it is noticeable that the gaps present between the CEP164C dots are filled with the TFK1 dots as observed on the top and side views (Fig. 2Ab,f) suggesting that TFK1 and CEP164C belong to two different compartments of the TF. In addition, this is supported by the fact that in PCF, the knockdown CEP164C RNAi does not affect the localization of TFK1 at the TFs (Fig. S8B).

Remarkably, colabelling with TY1::TbRP2 revealed a continuous radial arrangement of TbRP2 somewhat smaller and distinct from the nine-dot arrangement of TFK1 (Fig. 2Ac). In addition, the side views (Fig. 2Ag and Bd) confirmed that TbRP2 and TFK1 are on separate structures with TFK1 distal to TbRP2 (relative to the kinetoplast oriented downwards in Fig. 2 in the U-ExM images). At the early SK1N (early kinetoplast S phase) stage of the cell cycle, the BB and the maturation of the pro-BB are identified by BLD10 labelling (Fig. 2Bb). The U-ExM showed that TFK1 labelling is observed once the pro-BB matures. Indeed, the BLD10 labelling in Fig. 2Bb shows a newly maturing BB that is also associated with TFK1 labelling (indicated with an asterisk, Fig. 2Bb). This is confirmed by the TbRP2 labelling, which shows a newly TbRP2-positive structure associated with TFK1 labelling (Fig. 2Bd, asterisk) and TFK1 labelling (Fig. 2Bf, asterisk) close to the base of the presumed pro-BB MtQ labelled by BILBO1 (Broster Reix et al., 2021a), suggesting they could be markers for an event of maturation of the pro-BB.

Subsequent immunogold electron microscopy images of thin sections from detergent-extracted, pre-labelled, cytoskeletons using anti-TFK1 confirmed the precise location of TFK1 on the TF (Fig. 3). On longitudinal sections (micrographs A and B), the gold particles are observed at the tip of the TF region, at the base of the transition zone subtending the flagellum. This was clearly observed on transversal sections where the nine-bladed TF structures are radiating around the BB but the immunogold particles are distal to the blades (Fig. 3C,D). In order to determine the exact location, we measured the distance between the centre of the BB and the immunogold labelling on transversal sections revealing a length of 172±26 nm (mean±s.d., n=28, white arrow in Fig. 3C; Table S1). In addition, some immunogold labelling was observed close to a pro-BB suggesting that it has already entered maturation (Fig. 3D) in agreement with our above observation by U-ExM (Fig. 2Bb,d,f, indicated by an asterisk).

Taken together, our data indicate that TFK1 is a cytoskeleton-associated protein expressed in PCF and BSF parasites throughout the cell cycle. TFK1 is a marker of BB maturation, localizing at the tip of the TF, with a spatial organization that differs from those of the only other two *T. brucei* described TF proteins, CEP164C and TbRP2, as is schematized in Fig. 4.

The TFK1 CC1 coiled-coil domain is sufficient to target to the TF zone

To further characterize the three main regions of the TFK1 protein, we generated PCF cell lines tetracycline-inducible (Wirtz et al., 1999) for the ectopic expression of C-terminus 3×Myc-tagged TFK1 (TFK1::myc) and truncated forms of TFK1 (truncations T1 to T5 described in Fig. 5A) in the TFK1::HA background. The proteins were detected by immunofluorescence with anti-HA antibody for the endogenously tagged TFK1::HA and anti-Myc antibody for the ectopic copies (Fig. 5B; Fig. S5B), and with anti-Myc antibody by western blotting (Fig. S5A). The Myc-tagged proteins were all expressed after tetracycline induction (Fig. S5A). The expression of the ectopic proteins was induced with tetracycline for 24 h and the cells were subjected to immunofluorescence and western blotting (24 h and 48 h induction) (Fig. 5B; Fig. S5A,B). TFK1::myc colocalized with endogenously tagged TFK1::HA on detergent-extracted cytoskeletons (Fig. 5Bc) with no cytoplasmic pool as observed on whole-cell labelling (Fig. S5Bb). The truncations T1::myc (N-terminal domain) and T3::myc (IDR), both lacking the CC region were observed as a cytoplasmic pool in whole cells (Fig. 5Bd,f) that was not present in the detergent-extracted cytoskeleton (Fig. S5Bc,d), suggesting that they are not

Journal of Cell Science (2022) 135, jcs259893. doi:10.1242/jcs.259893

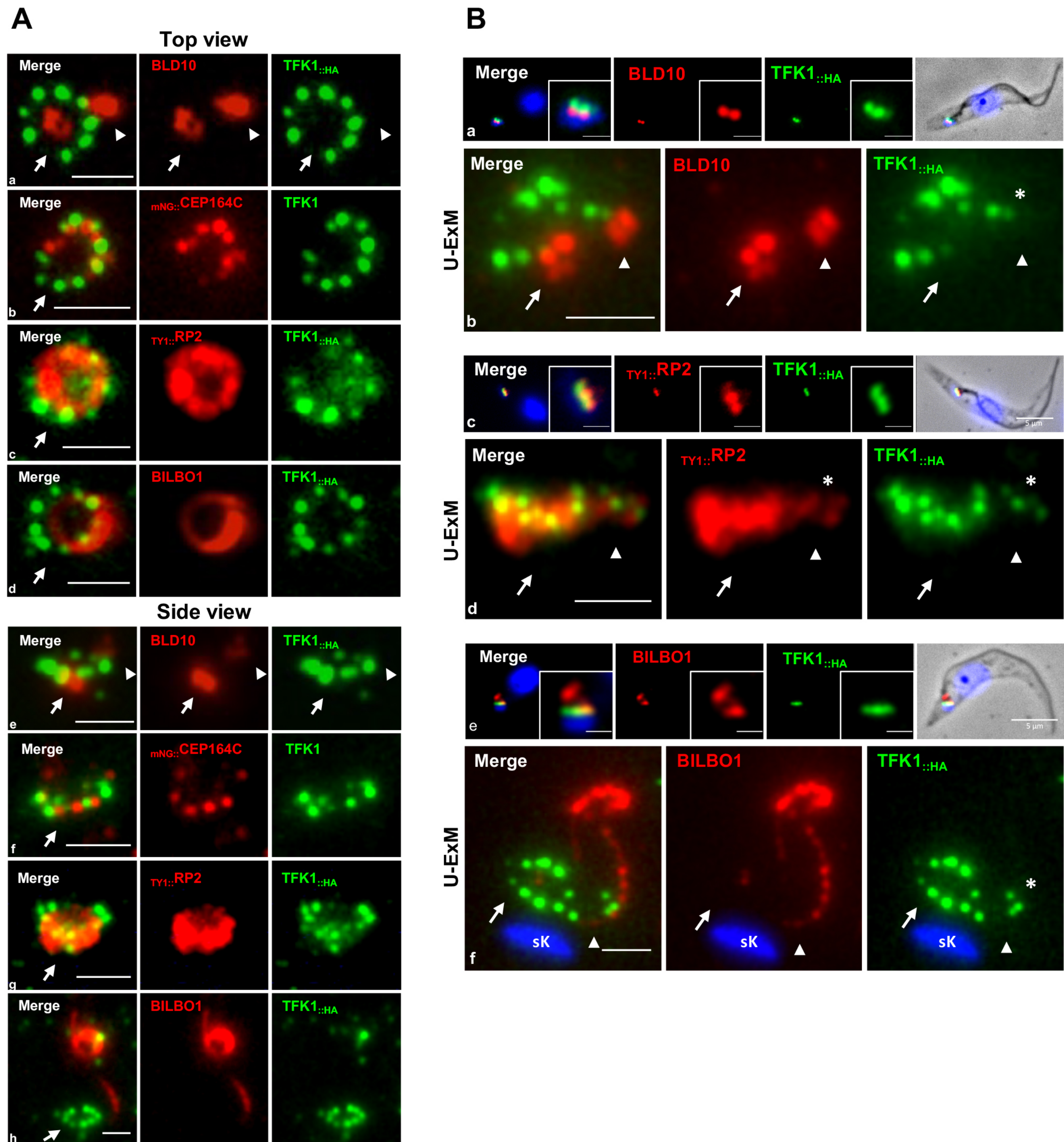

Fig. 2. TFK1, a newly identified TF protein and a marker of BB maturation. (A) Top (a–d) and side (e–h) views of U-ExM images showing the colabelling of TFK1 using anti-TFK1 in endogenously tagged TFK1::HA background PCF whole cells (green), and of BLD10 (a), mNG::CEP164C (b), TY1::RP2 (c) and BILBO1 (d) (red) in G1 stage cells. (B) Immunofluorescence (a,c,e) and U-ExM (b,d,f) on detergent-extracted cells showing the colabelling of endogenously tagged TFK1::HA (green) and BLD10 (red) (a,b), endogenously tagged TFK1::HA (green) and endogenously tagged TY1::RP2 (red) (c,d), endogenously tagged TFK1::HA (green) and BILBO1 (red) during pro-BB maturation in SK1N cells stage (early kinetoplast S phase) (e,f). The labelling on BB and pro-BB is indicated by an arrow and arrowhead, respectively, and the maturing pro-BB by an asterisk. U-ExM pictures (Ae–h and Bb,d,f) are oriented with the kinetoplast downwards. Scale bars: 5 µm (main images, A), 1 µm (inset, A); 2 µm (B). Expansion factor: 4.8 fold. Images shown are representative of three experiments.

required or sufficient for TF targeting. By contrast, the large CC domain (composed of CC1 and CC2; T2::myc) colocalized on the TF together with the endogenously tagged TFK1::HA on extracted cells (Fig. 5Be). To further uncover the exact region of the CC domain involved in the TF targeting, the CC1 (T4::myc) and CC2 (T5::myc) domains were expressed. Interestingly, we observed that the CC1 domain localized to TF (Fig. 5Bg) whereas the CC2 domain was observed in the cytoplasm in whole cells (Fig. 5Bh) and was not present in the detergent-extracted cytoskeleton (Fig. S5Be). These data show that the highly conserved coiled-coil domain CC1 (aa 75–536) is sufficient to target TFK1 to the TF.

The CC1 coiled-coil domain is involved in TFK1–TFK1 interaction

Because the CC and IDR domains can be involved in protein–protein interactions, we used the yeast two-hybrid (Y2H) approach

Journal of Cell Science (2022) 135, jcs259893. doi:10.1242/jcs.259893

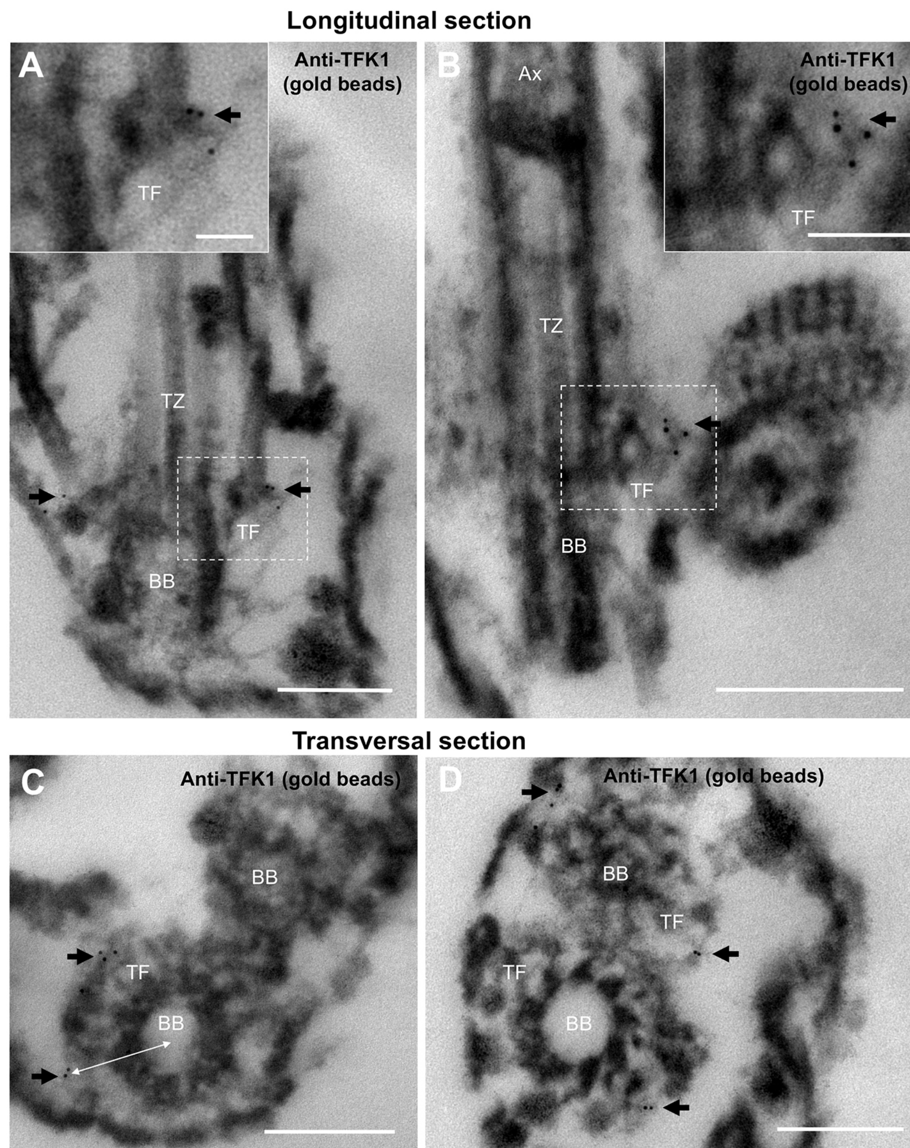

Fig. 3. TFK1 is localized at the tip of the TFs. Immunogold labelling on thin section of PCF whole cells showing the localization of TFK1 using anti-TFK1 (gold beads, black arrow). In A and B, views of longitudinal sections of the mature BB are shown. In C and D, views of transversal sections of the BBs are shown. Ax, axoneme. The white double-arrow in C indicates measurements of the distance of TFK1 to the centre of the BB. Scale bars: 200 nm (main images), 100 nm (insets). Images shown are representative of two experiments.

to determine whether they could be involved in TFK1–TFK1 interaction (Fig. 5C). Y2H assays demonstrated that TFK1 can form homodimers, as cell growth was obtained for full-length TFK1×full-length TFK1 (FL×FL, Fig. 5C). To identify which domain was involved in this interaction, the truncations T1 to T5 were tested against the full-length TFK1. Only the truncations T2 (CC1+CC2) and T4 (CC1) interacted with TFK1, demonstrating that the conserved coiled-coil domain CC1 (aa 75–536) is implicated in the formation of homodimers. However, we should take into account that *in vivo* the role of the CC1 domain in targeting to the TFs (Fig. 5Bg) could be a downstream result of the interaction of the CC1 domain with the endogenous full-length TFK1 protein. Interestingly, dimerization or oligomerization has been conceptualized for the recruitment of the CC-rich domain of human CEP164 to the centriole (Mennella et al., 2012; Yang et al., 2018).

TFK1 knockdown induces cell cycle arrest and cell death

To assess the function of TFK1, a tetracycline-inducible RNAi-mediated knockdown approach was used in the TY1::TFK1 background PCF and BSF cells (Wirtz et al., 1999). No phenotypes were observed in PCF over the time of RNAi induction despite the decrease of protein level observed by western blotting (Fig. S6A,B). However, absence of phenotypes might be due to incomplete depletion of TFK1 as the protein was still detected by western blotting after 96 h of induction (Fig. S6B). In contrast, in BSF cells, a growth arrest was observed 48 h post RNAi induction followed by cell death within 72 h (Fig. 6A). TFK1 protein level during RNAi induction was investigated by western blotting, and showed a strong decrease at 24 h post-induction and very low detection at 48 h post-induction using both anti-TY1 (left panel) and anti-TFK1 (right panel) antibodies (Fig. 6B). In addition, TFK1 protein depletion was also observed by immunofluorescence as the protein was not detected after 24 h of induction (Fig. 6C). Since TFK1 RNAi is lethal in BSF cells, we assessed cell cycle progression at different time-points of induction by using DAPI to stain the kinetoplast (K) and the nucleus (N) DNA and quantify their numbers (Fig. 6D). At 24 h post induction (+ Tet 24 h), the percentage of 1K1N cells decreased from 76% to ∼52%, together with an accumulation of 2K2N cells that increased from 8% to ∼22% (Fig. 6D, bottom panel). There was also appearance of abnormal cells such as 1K2N (∼3%), XKXN (X≥3) (∼8%) and

Journal of Cell Science

Journal of Cell Science (2022) 135, jcs259893. doi:10.1242/jcs.259893

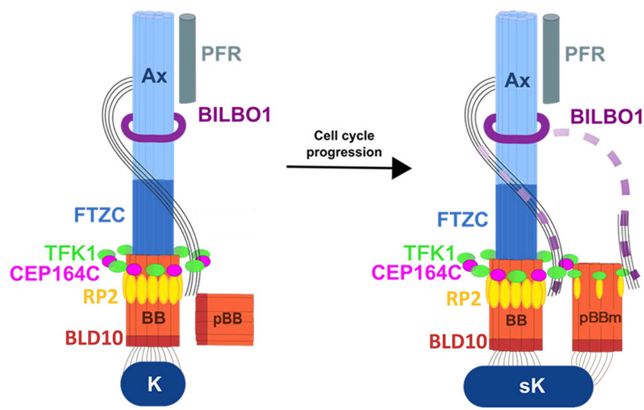

Fig. 4. Schematic representation of the subcellular localization of TFK1 together with key BB markers in *T. brucei*. Schematic representation showing the proposed model of TFK1 position in G1 stage (left scheme) and during the BB maturation stage (right scheme). Ax, axoneme; PFR: paraflagellar rod; BILBO1 (flagellar pocket marker); FTZC (transition zone marker); RP2 and CEP164C (TF markers); BLD10 (BBs marker); pBB: pro-basal body; pBBm, pro-BB maturation; K, kinetoplast; sK; kinetoplast in S phase.

'round' dead or dying cells (~3.4%) (Fig. 6D, top panel). Interestingly, the percentage of 2K2N cells at 48 h post induction (~9%) was similar to the non-induced 2K2N population (~8%) whereas the abnormal population of XKXN increased to ~43% (Fig. 6D, top panel) suggesting a downstream effect of the increase of the 2K2N cell population at 24 h of induction (~22%).

Overall, these results indicate that TFK1 is essential in BSF *T. brucei* and its depletion induces cytokinesis defects without affecting mitosis, leading to cells with an abnormal number of kinetoplasts and nuclei.

Knockdown of TFK1 affects cleavage fold completion leading to 'locked posterior–posterior' and 'tandem cell' phenotypes in BSF cells

To study further the phenotypes induced by TFK1 RNAi in BSF cells, and to preserve the morphology of the cells, including the cytoplasmic bridge, WT or TFK1 RNAi non-induced and induced cells were fixed in the culture medium, stained with DAPI and observed by phase contrast microscopy. The number of kinetoplasts (arrowheads) and nuclei (asterisks) were followed along the cell cycle stages for the non-induced cells (Fig. 7Aa). At the 2K2N stage (Fig. 7a, 2K2N, cytokinesis and abscission) cytokinesis progresses with the formation of a division cleft (dashed line) leading to the abscission stage, where the two daughter cells are connected with the cytoplasmic bridge (arrow) in a posterior end-to-posterior end manner. Finally, the bridge is broken by the flagellum-driven motility of both daughter cells (Wheeler et al., 2013). To investigate this division process during TFK1 depletion by RNAi, 24 h-induced cells were similarly prepared and observed, with a particular attention to the 2K2N cells (Fig. 7Ab,c). No phenotype was observed in the first cell cycle stages (1K1N, S1K1N and 2K1N). However, in the BSF 2K2N stage, two main cytokinesis defect phenotypes were observed, (1) an increase in a 2K2N cell population of cells that is connected by their posterior ends with a cytoplasmic bridge at the abscission stage, which we named the 'locked posterior-to-posterior' phenotype (from 17.6% in WT cells to 30.2% in induced cells) (Fig. 7Ab,d) and (2) an unusual KNKN organization, which we named the 'tandem cells' phenotype and was never observed in WT cells, which reached 13.4% of the 2K2N

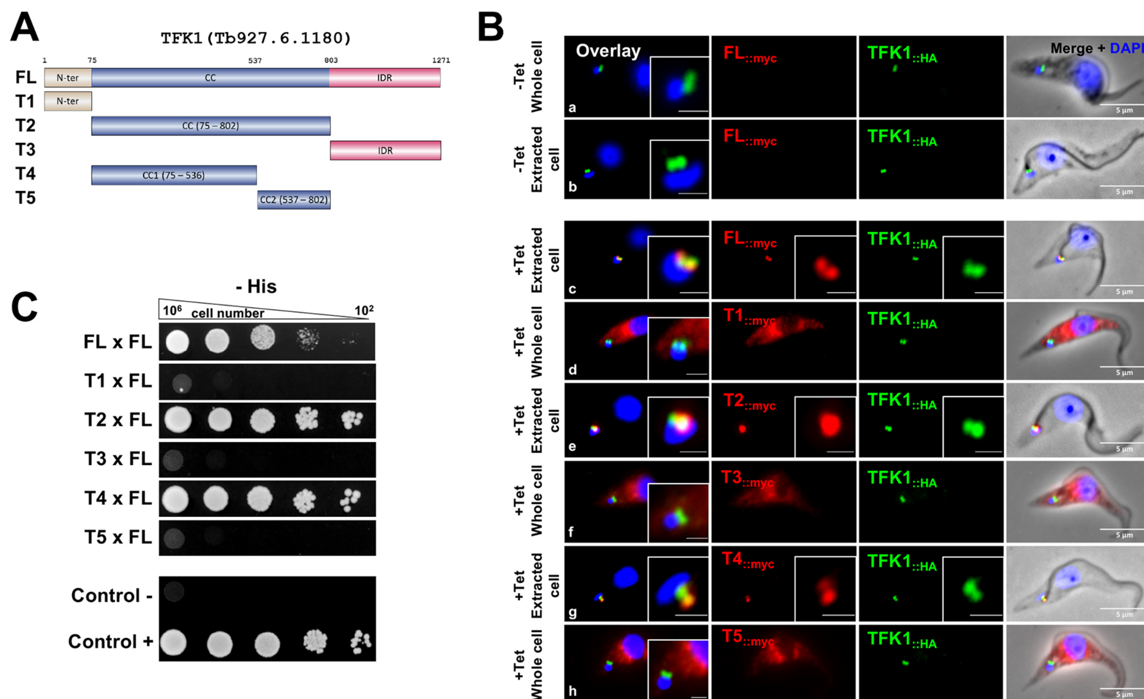

Fig. 5. Domain analysis of TFK1 shows key features. (A) Schematic representation of full-length TFK1 (FL) and truncations assessed (T1, N-ter aa 1–74; T2, CC aa 75–802; T3, IDR aa 803–1271; T4, CC1 aa 75–536; T5, CC2 aa 537–802). (B) Immunofluorescence labelling of TFK1::myc (red) in non-induced (a) and induced cells (b) and of truncations (T1::myc, T2::myc, T3::myc, T4::myc and T5::myc) (red) after 24 h of induction of expression in the endogenously tagged TFK1::HA background (green) PCF cells. Scale bars: 5 µm (main images), 1 µm (insets). (C) Yeast-two-hybrid assays on – histidine selective medium (–His) of full-length TFK1 and truncated forms of TFK1. The negative control (Control –) was lamin and T-antigen, and the positive control (Control +) was p53 and T-antigen. Images shown in B and C are representative of three and two experiments, respectively.

Journal of Cell Science (2022) 135, jcs259893. doi:10.1242/jcs.259893

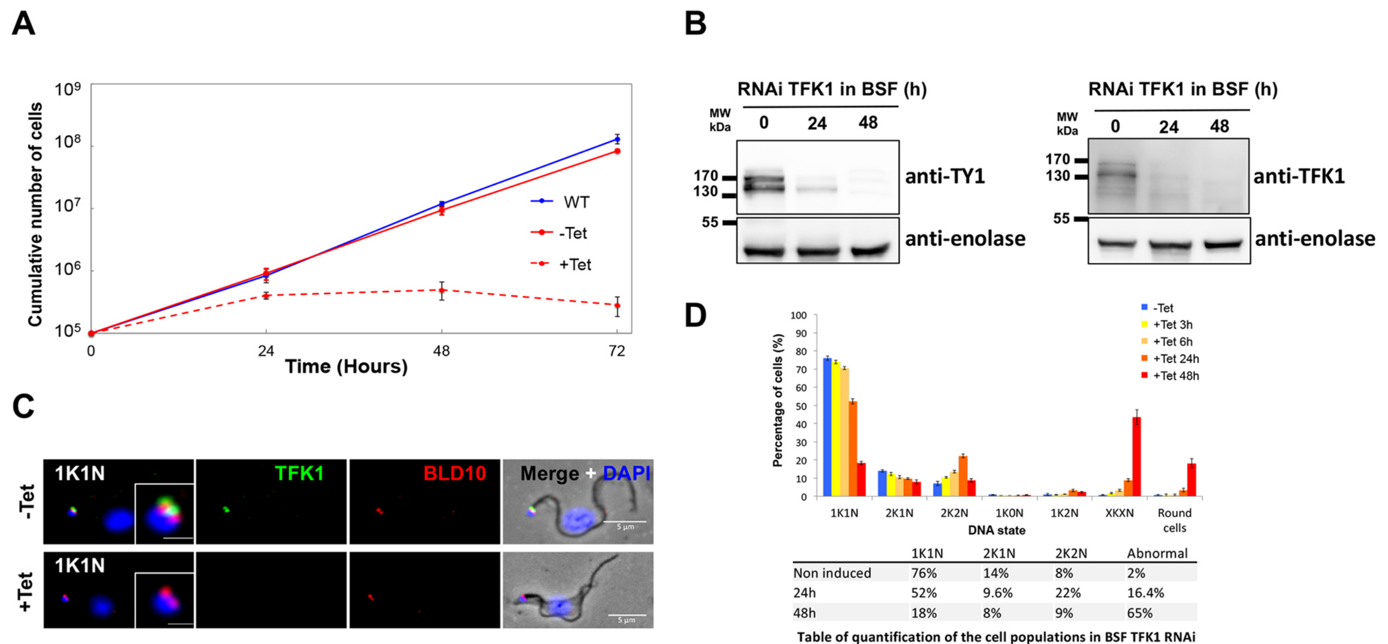

	1K1N	2K1N	2K2N	Abnormal
Non induced	76%	14%	8%	2%
24h	52%	9.6%	22%	16.4%
48h	18%	8%	9%	65%

Table of quantification of the cell populations in BSF TFK1 RNAi

Fig. 6. TFK1 is essential in bloodstream forms. (A) Growth curves of WT cells (blue line), non-induced cells (−Tet, red line) and tetracycline induced cells (+Tet, dashed red line) for TFK1 RNAi knockdown in BSF. Results are mean±s.e.m. (*n*=3). (B) Representative western blot analysis of the TFK1 protein level in endogenously tagged TY1::TFK1 BSF using anti-TY1 (left blot) and anti-TFK1 (right blot) before induction and 24 and 48 h post induction. The anti-enolase was used as loading control. (C) Immunofluorescence on detergent-extracted PCF cells, showing TFK1 (green) and BLD10 (red) before (−Tet) and 24 h post induction +Tet). Scale bars: 5 µm (main images), 1 µm (insets). Images shown in B and C are representative of three and four experiments, respectively. (D) Histogram of the nuclear and kinetoplast DNA content before the RNAi knockdown of TFK1 (−Tet) and 3 h, 6 h, 24 h and 48 h post induction induced in BSF TFK1 RNAi and table of quantification of the cell populations (abnormal cells including 1K2N, XKXN and round cells) (mean±s.e.m.; *n*>200, three independent experiments).

induced cell population (Fig. 7Ac,d). Therefore, the normal population of 2K2N cells, with a KKNN organization, decreased substantially (from 82.4% in WT cells to 56.3% in induced cells) (Fig. 7Aa,d).

In the locked posterior-to-posterior phenotype, TFK1 RNAi-induced BSF cells progressed normally through the cell cycle up to the abscission step. At the 2K2N stage an apparently proper fold and two nascent posterior ends were formed in the 2K2N cells (Fig. 7Ab, 2K2N cytokinesis), and these cells showed a correct furrow ingression and pre-abscission as seen by the presence of a cytoplasmic bridge in a posterior-to-posterior organization (Fig. 7Ab, 2K2N no abscission). However, these cells were not able to complete abscission before asynchronous mitosis cycles occurred as shown by the number of DAPI-stained kinetoplasts and nuclei (Fig. 7Ab, XKXN no abscission). Both attached daughter cells were asynchronous with an unequal number of flagella as visualized by PFR labelling (Fig. 7Ce,f). Scanning electron microscopy (SEM) analysis supported these observations, showing two daughter cells connected by their posterior ends (Fig. 7D, arrows, locked posterior-to-posterior).

In the previously undescribed 2K2N tandem cells phenotype, the organization of the kinetoplasts and nuclei resembles that seen in PCF cells with a KNKN distribution instead of a KKNN distribution (Fig. 7Ac, 2K2N). This cell population was never observed in non-induced cells but represented 13.4% of the 2K2N population of 24 h-induced TFK1 RNAi cells (Fig. 7Ad, tandem cells). The observation of these cells after detergent extraction showed in more detail that the sub-pellicular microtubule cytoskeleton of both WT and tandem cells form a continuous corset for the two daughter cells (Fig. 7B). However, the tandem cells have a clearly misplaced new kinetoplast and new flagella (Fig. 7B, +Tet). This could lead to or be the result of abnormal fold positioning (Fig. 7B, +Tet) compared to in the non-induced condition (Fig. 7B, −Tet), where the fold terminates closer to the posterior end in BSF cells and defines the two nascent posterior ends (Wheeler et al., 2013). In induced cells, the DNA of the two cells continued to replicate, indicating a restart in cell cycle and leading to XKXN and multi-flagellated cells, as shown with the flagella labelling with the anti-PFR antibody (Fig. 7Cb,c), without achieving cytokinesis (Fig. 7Ac XK2N, XKXN). Interestingly, whole-cell and cytoskeleton preparations revealed the existence of a structure resembling a bridge that prevented daughter cell separation (Fig. 7Ac, arrows XNXN; Fig. 7Cc). Similar observations were made by SEM, showing this atypical organization of tandem cells in BSF (Fig. 7D, arrows tandem cells).

In TFK1 RNAi-induced cells, neither defects in the BBs (as labelled with anti-BLD10) (Fig. S7Ab) nor in flagellum structure (as observed on thin section by electron microscopy) were observed (Fig. S7Ab). Likewise, the cytoskeleton-associated structures, such as the flagellum (visualized by a PFR signal, Fig. 7C) and the FAZ (labelled with the anti-FAZ L3B2 monoclonal, Fig. 7C), and the flagellar pocket collar (labelled with anti-BILBO1, Fig. S7Ad,Ba,c), were unaffected by TFK1 knockdown. Comparison of electron microscopy images of thin sections from non-induced and 24 h-induced TFK1 RNAi BSF cells showed no obvious difference in the overall ultrastructure of the cytoskeleton (Fig. S7B). PFR length was also measured in non-induced and induced TFK1 RNAi conditions, which showed no change in the length of the flagella, suggesting a proper flagellum formation (Fig. S7C). We also compared the diameter of the TF area after TFK1 RNAi knockdown by measuring the distance between the two sides of the FP at the base of the flagella (indicated by a white double-arrow on Fig. S7Bc), but this showed no significant differences between induced and non-induced cells (Fig. S7D). Furthermore, on cells induced for the

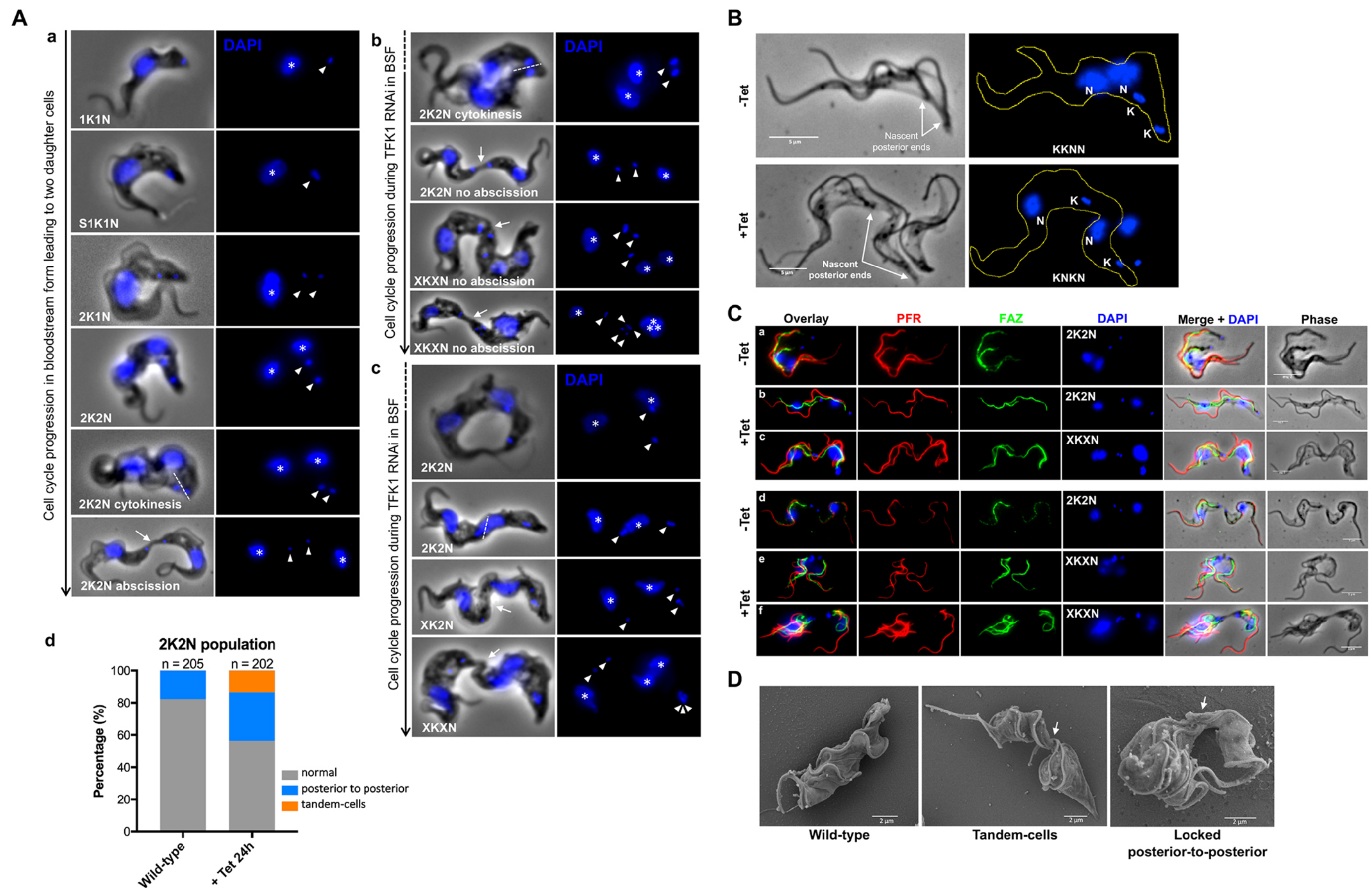

Fig. 7. TFK1 knockdown in BSF leads to cytokinesis defects. (A) DAPI staining on whole cells before (a) and after TFK1 RNAi knockdown (b,c) showing cell cycle progression [position of division fold generation, dashed line; nucleus (asterisk); kinetoplast (arrowheads); fold (dashed line); cytoplasmic bridge (arrow)]. (d) Quantification of the 2K2N cell populations in wild-type population and in 24 h post induction of TFK1 RNAi knockdown population. Normal stage (grey bar), cells in pre-abscission stage in 'posterior-to-posterior' organization (blue bar), and 'tandem cells' forming abnormal KNKN organization (orange bar). (B) Detergent-extracted cell cytoskeletons coupled with DAPI staining before (–Tet) and 24 h after (+Tet) TFK1 RNAi knockdown. (C) Immunofluorescence on detergent-extracted cells showing the FAZ (flagellar attachment zone, green) and PFR (paraflagellar rod, red) labelling before (–Tet) and 24 h post induction (+Tet), which leads to the tandem cells phenotype (b,c), and the cells locked in the posterior-to-posterior phenotype (e,f). Scale bars: 5 µm. (D) SEM analysis showing a 2K2N wild-type cell (left) and TFK1 RNAi phenotypes after 24 h induction [tandem cells (centre) and cells in locked posterior-to-posterior organization (right)]. The arrows indicate the cytoplasmic bridge. Images shown are representative of two to five experiments.

RNAi knockdown of the flagellar pocket collar protein BILBO1, which display a detached new flagellum and no FP biogenesis (Bonhivers et al., 2008), TFK1 labelling remains present at the BB (Fig. S8A). This suggests that absence of FP formation does not affect the localization, and most probably, the function of TFK1.

Taken together, our data demonstrate that TFK1 is a TF protein. Colocalization of TFK1 with CEP164C and TbRP2 suggest that TFK1 is the first TF matrix protein identified in trypanosomes, and that it is essential for the final stages of the cell cycle of the *T. brucei* BSF (localization schematized in Fig. 8). Depending on the stage of progression in the cell cycle, TFK1 knockdown leads (1) to a misplacement of the new BB resulting in a KNKN phenotype that we named 'tandem cells' that has not been reported previously in BSF, and (2) to a defect in the abscission that has previously been described in PCF cells for other cell cycle proteins (Sinclair-Davis et al., 2017).

DISCUSSION

Trypanosome BBs act as vital master organizers of the cytoskeleton, organelles and flagellum positioning (Lacomble et al., 2009, 2010). During maturation, the pro-BB acquires appendages, essential structures for docking to the plasma membrane and recruitment of the IFT proteins (Stephan et al., 2007; Morga and Bastin, 2013; Wei et al., 2015; Bertiaux et al., 2018). These radial structures are comprised of nine distal appendages (DAs) and transition fibres (TFs) and nine sub-distal appendages (SDA) (Tanos et al., 2013; Vaughan and Gull, 2016; Garcia-Gonzalo and Reiter, 2017; Trépout et al., 2018; Yang et al., 2018). In this study, we identified transition fibre protein kinetoplastid specific-1 (TFK1) as a novel TF component and BB maturation marker that is unique to the Kinetoplastea class and present throughout the trypanosome cell cycle in PCF and BSF.

TFK1, a component of the distal appendage matrix in the TFs

Only two TF proteins have been described in *T. brucei*, TbRP2 and CEP164C (Andre et al., 2014; Atkins et al., 2021; Stephan et al., 2007). Using U-ExM, we show for the first time in *T. brucei* the high resolution localization of CEP164C, which adopts a radial arrangement of several dense dots similar to the labelling observed for human CEP164 (Yang et al., 2018), and of TbRP2 that is proximal to CEP164C. We show here that TFK1 is localized at the BB, is distal to TbRP2 and is organized as nine equidistant dots around the BB that fill the circumferential gaps of CEP164C arrangement without colocalization. Together with CEP164C and TbRP2, TFK1 is the third bona fide protein component of the trypanosome TFs.

Journal of Cell Science (2022) 135, jcs259893. doi:10.1242/jcs.259893

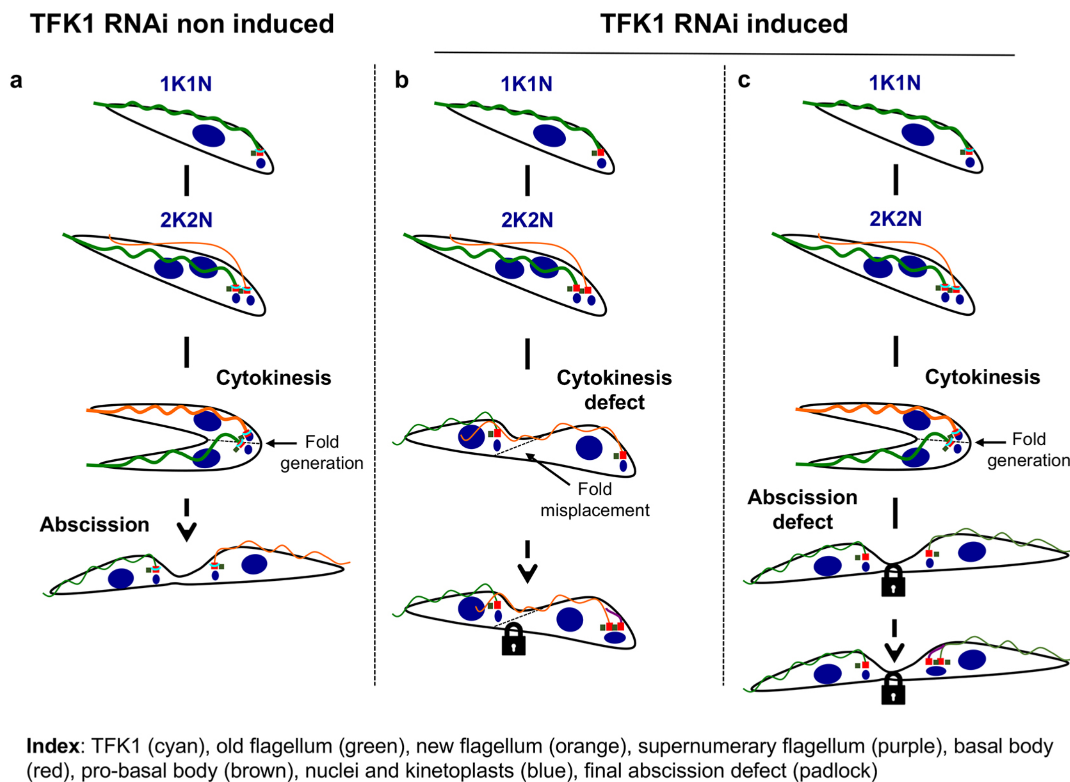

Index: TFK1 (cyan), old flagellum (green), new flagellum (orange), supernumerary flagellum (purple), basal body (red), pro-basal body (brown), nuclei and kinetoplasts (blue), final abscission defect (padlock)

Fig. 8. Schematic representation of the TFK1 knockdown leading to a deregulation of the cell division. (A) Representation of a normal cell cycle division in BSF cells. (B,C) Abnormal division leading respectively to tandem cells and locked posterior-to-posterior cell phenotypes.

Recent ultrastructural studies of the human TFs/DAs described in great details a cone-shaped architecture composed of nine distal appendage blades (DABs) that are embedded in the distal appendage matrix (DAM), also known as periciliary diffusion barrier (PCB) (Nachury, 2018), where FBF1 and IFT molecules localize (Yang et al., 2018). Our measurements reveal that the nine TFK1 dots define an inner and an outer diameter of 356±28 nm and 558±58 (mean±s.d.), respectively, similar to the diameters found for the human orthologs CEP164 (568±18 nm to 219±14 nm) and FBF1 (269±33 nm to 496±26 nm) on the DAs (Yang et al., 2018; Bowler et al., 2019; Katoh et al., 2020). Taken together, our data suggest that TFK1 might be present in the DAM structure, similar to the FBF1 protein between the nine DABs composed of, among others, CEP164 (Yang et al., 2018). In addition, we show that the TFK1 immunogold labelling is located at 172±26 nm away from the centre of BBs, in agreement with the same distance of ∼177 nm measured for mammalian centrioles (Bowler et al., 2019). This distance (or radius) is equivalent to a diameter of 344±51 nm. The diameter of the dense TF structures (the blades) observed in *T. brucei* by electron microscopy (EM) is in the range of 338 nm to 388 nm (Trépout et al., 2018), suggesting that TFK1 localizes at the distal end of the blades structure in the DAM as described for FBF1 (Wei et al., 2013; Yang et al., 2018).

We show, in BSF, that depletion of TFK1 does not affect BB structures per se, flagella structure and length or the diameter of the TF area, indicating that TFK1 is not involved in the biogenesis of these cytoskeletal structures. In comparison, Atkins and colleagues have shown that RNAi of CEP164C, in PCF cells, induces abnormal elongation of the old flagella, without altering its structure (Atkins et al., 2021). Within the same RNAi strain, we show that, when CEP164C is depleted, TFK1 protein is still detected at the TF (Fig. S8B). These results indicate that although the two proteins CEP164C and TFK1 are close on the TF, TFK1 localization is independent of CEP164C. This is similar to what is seen upon the absence of the human CEP164 at the DAB tips, which did not affect the recruitment of FBF1 to the DAM (Yang et al., 2018), indicating that CEP164 has a distinct role from other central components of the DAB (Yang et al., 2018). FBF1 is a DAM protein required for ciliogenesis, ciliary gating, centriole duplication and separation (Inoko et al., 2018; Tanos et al., 2013; Wei et al., 2013; Yang et al., 2018). Using BLAST-P, we searched for the FBF1 (isoform 1) human protein sequence (Q8TES7-1) ortholog in kinetoplastids and identified Tb926.6.4100 (Protein ID: XM_840435.1) with 11.6% similarity and 7.2% identity. Interestingly, Tb926.6.4100 has been localized at the BBs by the TrypTag resource (Dean et al., 2016, 2017). The DAM area could be composed of different proteins that play different functions, specific to the organism.

TFK1 is involved in furrow function in the BSF cell cycle

In BSF, TFK1 depletion induced a misregulation of the cell division cycle characterized by an arrest of cytokinesis at 2K2N stage leading to either a previously uncharacterized ‘tandem cells’ phenotype, with a KNKN arrangement along the posterior to anterior of the cell axis, or a ‘locked posterior-to-posterior’ phenotype (NKKN), which corresponded to an abscission arrest or delay leading to rapid cell death. Nevertheless, in both phenotypes, mitosis still occurred. However, no phenotype was observed in PCF RNAi cells. It is well documented that depletion of proteins involved in structural integrity and/or flagellum motility induces major defects in cytokinesis, which are frequently lethal in BSF cells (Broadhead et al., 2006; Ralston et al., 2006; Dacheux et al., 2012; Wheeler et al., 2013; Dang et al., 2017; Zhang et al., 2019). In addition, and confirming an important phenomenon observed by us, several studies show that RNAi knockdown of the same protein can produce

Journal of Cell Science

different phenotypes in PCF and BSF life stages (Hammarton et al., 2003; Kumar and Wang, 2005; Broadhead et al., 2006; Benz et al., 2012; Zhang et al., 2019; Lai et al., 2021; Morriswood et al., 2009; Broster Reix et al., 2021b). Our data demonstrate once again that the essentiality of a protein, such as TFK1 can vary from one life-cycle stage to another in *T. brucei*.

Interestingly, the TFK1 RNAi 'tandem cells' phenotype obtained in BSF show the same KNKN arrangement of WT, PCF cells suggesting a role for TFK1 in BB placement. During the elongation of the new flagellum in BSF, the distal tip is connected to the cell body plasma membrane in the groove structure, which is present until the new flagellum extends beyond the anterior end of the cell (Hughes et al., 2013). The initiation of the division fold and the cleavage furrow corresponds to the resolving of the groove and to a significant reduction of the distance between the two kinetoplasts (Hughes et al., 2017; Tyler, 2001). In the KNKN tandem cells phenotype, the new and old FAZ and the flagella grew properly, but a stopping point for the elongation of the sub-pellicular microtubule corset and the separation of the flagella seemed to be missing, as well as a starting point for the initiation of the cleavage furrow (Absalon et al., 2007; Davidge et al., 2006; Farr and Gull, 2012; Hughes et al., 2017; Robinson et al., 1995).

The exact molecular role of TFK1 is yet to be discovered but TFK1 together with TbRP2 were identified by proximity-dependent biotinylation identification (BioID) as an interactor protein of TOEFAZ1 (also known as CIF1; a key regulator of the cytokinetic furrow) but not CEP164C (Hilton et al., 2018). However, our Y2H assays did not show a direct interaction between TFK1 and TOEFAZ1 (Fig. S8C) suggesting that TOEFAZ1 comes in close proximity to TFK1 during its journey along the flagellum (McAllaster et al., 2015; Sinclair-Davis et al., 2017; Zhou et al., 2016a) but do not interact. Moreover, TFK1 has been identified in the proteomic analyses of the immuno-isolated bi-lobe complex (Gheiratmand et al., 2013). Gheiratmand and colleagues have identified many other proteins localized on single-copy organelles, such as the flagellum, the MtQ, the FPC, the kinetoplast, and the bi-lobe but neither TbRP2 nor CEP164C were identified in their analysis. This suggests that TFK1 could have a specialized role interacting with some proteins that transit along the MtQ towards the bi-lobe and beyond.

Our study also shows that TFK1 depletion induces the blockage or delay of abscission, leading to the 'locked posterior-to-posterior' phenotype, while allowing further rounds of mitosis.

TFK1, a candidate regulator of cytokinesis in bloodstream form

The studies of the trypanosome-specific key regulators (TOEFAZ1, CIF2, CIF3, KLIF and FRW1) in the initiation of cytokinesis in *T. brucei* have shown that they are regulated by different mechanisms at different stages of the life cycle (BSF and PCF) (Zhou et al., 2016a,b; Zhou and Li, 2016; Hilton et al., 2018; Zhou et al., 2018). The two trypanosome-specific proteins KLIF and FRW1 are remarkable examples. Both were identified at the cell division fold and cleavage furrow (Hilton et al., 2018; Zhou et al., 2018). Although these two proteins are expressed in both forms, KLIF is essential in PCF and FRW1 is essential in BSF (Hilton et al., 2018; Zhang et al., 2019). FRW1 is localized at the BBs and at the furrow ingression during cytokinesis but its depletion was not essential for survival in PCF. In contrast, in the BSF, FRW1 has been detected as multiple punctate dots in the middle portion of the cells and its depletion leads to defects in cytokinesis initiation and is lethal (Zhang et al., 2019). The common underlying mechanism between the phenotypes induced during the RNAi of TFK1 and of FRW1 could be the modification of the corset at a specific time point. This would first allow the initiation of the groove ingression, which could be affected in the tandem cell phenotype, and second, allow the cytoplasmic bridge to be cut, which would no longer occur or be delayed in the locked posterior-to-posterior phenotype. The essential role of the centriole in cytokinesis and especially in the regulation of abscission has been described in mammalian cell lines. Migration of the centriole to the intercellular bridge (midbody) controls the release of microtubules and the completion of cell division. The authors suggest that this centrosome-dependent pathway might have been conserved during evolution (Jonsdottir et al., 2010; Piel et al., 2001). The centriole and BB clearly have other, cryptic functions that to date have not clearly been elucidated.

In summary, our results describe TFK1 as a kinetoplastid-specific protein and as a mature and maturing BB marker, localized on the TFs. TFK1 is the third component of the TF region, with TbRP2 and CEP164C, in *T. brucei*. TFK1 is displayed in a typical radial arrangement in the distal appendage matrix, as nine dense points between the molecules of CEP164C. TFK1 is essential for BSF cells, but not PCF cells. Its depletion induces, on one hand, the absence of furrow associated with segregation of BBs similar to that of PCFs (KNKN) and, on the other hand, leads to the blockage of abscission during cytokinesis in BSFs. These two processes might be interlinked or have some degree of interdependency. Our results suggest an essential role of TFK1 in the segregation and positioning of BBs to ensure the shape of subsequent daughter cells. The role of TFK1 could be extended to other forms of the trypanosome life cycle, which exhibit different morphologies (trypomastigote and epimastigote) as well as a different positioning of the nucleus and BBs along the axis of the cell (Langousis and Hill, 2014; Varga et al., 2017; Zhang et al., 2019; Lemos et al., 2020).

MATERIALS AND METHODS

In silico analysis

The TrypTag resource (http://tryptag.org) (Dean et al., 2016) previously identified Tb927.6.1180 (ProteinID: XP_845240.1) as a BB protein. TFK1 orthologs were identified by walking BLAST-P, PSI-BLAST and HMMER (Altschul, 1997; Altschul et al., 2005, 2005; Finn et al., 2011) using default parameters [standard databases, non-redundant protein sequences database, maximum target sequences 100, with short queries, expect threshold E-value of 0.05 (and 0.01), no maximum matches in a query range]. Multiple sequence alignments using ClustalOmega identified three main regions where residues are conserved among the TFK1 orthologs (Madeira et al., 2019). Accession numbers of protein sequences used are: *Trypanosoma brucei* (XP_845240.1, Tb927.6.1180), *Trypanosoma brucei gambiense* (XP_011773895.1, Tbg972.6.880), *Trypanosoma congolense* (CCC90840.1, TcIL3000_6_680), *Trypanosoma cruzi* (PWV00945.1, TcCLB.507603.120), *Trypanosoma vivax* (CCC48277, TvY486_0600680), *Leishmania major* (Q4QGT1, LmjF.12.0120), *Phytomonas* sp. (CCW65273.1, GSEM1_T00005970001), *Crithidia fasciculate* (CFAC1_010006900, CFAC1_06_0150Z). InterPro provided functional analysis primary and secondary structures of proteins (https://www.ebi.ac.uk/interpro/; Blum et al., 2021).

Trypanosome cell lines, culture and transfection

Procyclic (PCF) cell line SmOx P427 (Poon et al., 2012) was grown in SDM-79 medium (GE Healthcare, G3344-3005) pH 7.4 supplemented with 2 mg/ml hemin (Sigma Aldrich, H-5533), 26 µM sodium bicarbonate, 10 mM D-glucose, 3.5 mM L-glutamine, 5.3 mM L-proline, 0.9 mM sodium pyruvate, 3.4 mM L-threonine, 150 mM glutamic acid, 120 µM sodium acetate, 230 µM D-glucosamine, 10% fetal calf serum complement-deactivated at 56°C for 30 min (FBS; Gibco, 11573397), 1 µg ml^{-1}

puromycin and incubated at 27°C. Bloodstream (BSF) cell line SmOx B427 (Poon et al., 2012) was cultured in Iscove's modified Dulbecco's medium (IMDM) containing 10% fetal calf serum complement-deactivated at 56°C for 30 min (FBS; Gibco, 11573397), 36 mM sodium bicarbonate, 136 µg ml^{-1} hypoxanthine, 39 µg ml^{-1} thymidine, 110 µg ml^{-1} sodium pyruvate, 28 µg ml^{-1} bathocuproine, 0.25 mM β-mercaptoethanol, 1.7 mM L-cysteine, 62.5 µg ml^{-1} kanamycin, 0.1 µg ml^{-1} puromycin and incubated at 37°C with 5% CO_2. For transfection, cell lines were grown at $5{\times}10^6$–$10{\times}10^6$ cells/ml, then $3{\times}10^7$ cells were electrotransfected using transfection buffer as previously described (Wirtz et al., 1999; Schumann Burkard et al., 2011) with 10 µg of linearized plasmid using NotI or PCR product using the program X-001 of the Nucleofector®II, AMAXA apparatus (Biosystems).

After transfection, clones were obtained by serial dilution and maintained in logarithmic phase growth at $2{\times}10^6$ cells ml^{-1} for PCF and at 10^5 cells ml^{-1} for BSF. Selection antibiotics were added to the media according to the transfected product. Phleomycin (5 µg ml^{-1} for PCF and 2.5 µg ml^{-1} for BSF) was added to the medium of transfected cells to select for those harbouring the pLew100-3cMyc and p2T7tiB constructs, blasticidin (20 µg ml^{-1} for PCF and 10 µg ml^{-1} for BSF) and hygromycin (25 µg ml^{-1} for PCF and 5 µg ml^{-1} for BSF) were added to select the transfected cells harbouring endogenous tags using pPOT vectors (Dean et al., 2015). Gene expressions and RNAi induction in the parasites were induced with tetracycline at 10 µg ml^{-1}. Growth curves representing logarithmic number of cells were calculated by counting the number of cells every 24 h using Mallassez counting chamber slides.

Plasmid construction

E. coli BL21 (DE3) expression vectors

To produce the anti-TFK1 mouse monoclonal antibody, the TFK1 open reading frame was amplified from *T. brucei* 927 genomic DNA (Melville et al., 2000) and cloned between HindIII and BamHI restriction sites into pET28a+ (Novagen) in frame with a C-terminus 6-histidine tag.

Trypanosome vectors

To express the full-length TFK1 (aa 1–1271) and its truncations (T1, aa 1–74; T2, aa 75–802; T3, aa 803–1271; T4, aa 75–536; T5, aa 537–802) in PCF, the fragments were amplified by PCR and cloned into HindIII and NdeI restrictions sites of the pLEW100-X-3cMyc in frame with the C-terminus 3×Myc tag (modified in-house from Wirtz et al., 1999). For the RNAi experiments in PCF and BSF, the TFK1 corresponding fragment (466–976 bp) was cloned between XbaI and XhoI restriction sites of the twin promoters plasmid p2T7tiB (LaCount et al., 2002). For endogenous gene tagging, primers were designed as described in Dean et al. (2015) and PCR was performed using pPOTv4 (for N-terminus 10-TY1 tagging, Blasticidin resistance) or pPOTv7 vector (for C-terminus 3-HA tagging, hygromycin resistance) as template. The PCR product was then used for trypanosome transfection as described in Dean et al. (2015).

Yeast two-hybrid vectors

To express the full-length TFK1 (aa 1–1271) and its truncations (T1, aa 1–74; T2, aa 75–802; T3, aa 803–1271; T4, aa 75–536; T5, aa 537–802) in yeast for interaction test, the fragments were amplified and cloned into SmaI and BamHI restriction sites of the pGAD-T7 (activating domain, Clontech) and into BamHI and NcoI restriction sites of the pGBK-T7 (binding domain, Clontech).

Western blot analysis

Trypanosomes were collected, centrifuged at 1000 ***g*** (PCF) or 800 ***g*** (BSF) for 10 min, and washed in PBS for PCF cells, and Voorhei's modified PBS (vPBS; 136.9 mM NaCl, 3 mM KCl, 16 mM Na_2HPO_4, 3 mM KH_2PO_4, 45.9 mM sucrose, 10 mM glucose) for BSF cells. For whole cells, the number of cells to be loaded per well were calculated, then re-suspended in 2× Laemmli buffer (Laemmli, 1970), plus 250 IU ml^{-1} nuclease (Sigma Aldrich, ref. E1014). For detergent-extracted cells (cytoskeletons), cells were washed and re-suspended in 1% NP40, 100 mM PIPES pH 6.9, 1 mM $MgCl_2$ for 7 min. Cytoskeletons were checked by microscopy, then centrifuged at room temperature for 10 min at 1000 ***g***, washed in 100 mM PIPES pH 6.9, 1 mM $MgCl_2$ and resuspended in 2× Laemmli buffer. The samples were boiled at 100°C for 5 min then stored at −20°C until required. 10% SDS-PAGE gels were prepared and samples loaded at $5{\times}10^6$ PCF or BSF trypanosome cells per well, according to the experiment. Samples were separated according to manufacturer's recommendations then transferred in a semi-dry system (Bio-Rad Trans-Blot Semi-dry transfer cell 221BR54560) onto PVDF membrane and incubated with blocking solution (BS; 5% skimmed milk powder, 0.2% Tween-20 in TBS) for 1 h. For detection of tagged and non-tagged protein expression in trypanosomes, an anti-tag antibody or an antibody against the native protein was diluted in blocking solution according to the recommendation and incubated with the membranes overnight at 4°C. Membranes were washed in TBS and then in BS before probing with a specific secondary antibody conjugated to horseradish peroxidase (HRP) for 60 min at room temperature (RT). The following antibodies were used as primary antibodies: anti-TFK1 (mouse monoclonal IgG1 purified, 1:500), anti-HA (mouse monoclonal IgG1, Biolegend, 901513, 1:1000), anti-TY1 (BB2 mouse monoclonal antibody IgG1, 1:100; Bastin et al., 1996) and anti-c-Myc (rabbit polyclonal, Sigma, C-3956, 1:1000). Anti-enolase (rabbit polyclonal, 1:70,000; Hannaert et al., 2003) and anti-tubulin (TAT1 mouse monoclonal, 1:1000; Woods et al., 1989) were used as loading controls. The secondaries used were anti-mouse-IgG conjugated to HRP, diluted 1:10,000 in BS (Jackson, sheep, 515-035-062) and anti-rabbit-IgG conjugated to HRP, diluted 1:10,000 in BS (Sigma, goat, A9169). Revelation was carried out using Image Quant LAS 4000 (GE) or Chemidoc (Biorad).

Immunofluorescence assays

1 ml of log-phase PCF cells were centrifuged for 10 min at 1000 ***g***, washed in 1× PBS, then 30 µl was loaded onto slides coated with poly-L-lysine 0.1% solution (Sigma-Aldrich, P8920) for 5 min to adhere. Whole cells were fixed in methanol at −20°C for at least 30 min. Cytoskeleton extraction was carried out with 0.25% NP40 (Igepal) in PIPES buffer (100 mM PIPES pH 6.8, 1 mM $MgCl_2$) for 5 min, washed twice in PIPES buffer and cytoskeletons were fixed with methanol as described in Florimond et al. (2015). For BSF, 10 ml of log-phase cells were collected, centrifuged at 800 ***g*** for 10 min, then washed in vPBS; whole cells were fixed in 2% formaldehyde directly in the medium for 10 min and then loaded onto slides coated with poly-L-lysine 0.1% solution (P8920 Sigma-Aldrich) for 5 min to adhere and permeabilized by methanol immersion for 5 min (Wheeler et al., 2013). Cytoskeleton extraction was carried out with 0.25% NP40 (as described above). Fixed cells were then incubated for 1 h with single or combination of antibodies diluted in PBS plus 2% BSA. Anti-HA mouse monoclonal antibody IgG1 (Biolegend, 901513, 1:1000), anti-HA mouse monoclonal antibody IgG2a (Genetex, GTX628902, 1:1000) and anti-TY1 BB2 mouse purified monoclonal antibody IgG1 (1:1000) (Bastin et al., 1996) were used as antibodies against tagged proteins, anti-cMyc (rabbit polyclonal, Sigma, C-3956, 1:1000) to detect overexpressed proteins, anti-TFK1 mouse monoclonal purified antibody IgG1 was used to detect the native TFK1 protein (1:500), anti-BLD10 (1:1000) (Dang et al., 2017) were used as pro- and mature BB markers, anti-FTZC rabbit polyclonal antibody (1:10,000; Bringaud et al., 2000) was used as a transition zone marker, anti-*Tb*BILBO1 rabbit polyclonal (against aa 1–110, 1:4000; Florimond et al., 2015), anti-PFR2 rabbit polyclonal antibody (1:200; Kohl et al., 1999), anti-FAZ mouse monoclonal antibody L3B2 (1:1000; a kind gift from Keith Gull, University of Oxford, UK; Kohl et al., 1999), anti-mNeonGreen (rabbit polyclonal, Ximbio, 155278, 1:10,000), washed twice in PBS plus 0.1% Tween 20, then incubated 1 h with the appropriate secondary antibodies diluted 1:100 in PBS plus 2% BSA: anti-mouse-IgG FITC-conjugated (Jackson, 115-095-164), anti-rabbit-IgG Alexa Fluor 594-conjugated (Molecular Probes, A-11012), anti-mouse-IgG1 Alexa Fluor 594-conjugated (Molecular Probes, A-21125), and anti-mouse-IgG2a Alexa fluor 488-conjugated (Molecular Probes, A21131). Kinetoplasts and nuclei were stained with 10 µl DAPI (10 µg/ml) in 1× PBS for 5 min and slides were mounted with Slowfade® Gold antifade reagent (Molecular Probes). Images were acquired on a Zeiss Imager Z1 microscope with Zeiss 100× oil objective (NA 1.4), using a Photometrics Coolsnap HQ2 camera and Metamorph software (Molecular Devices) and processed with ImageJ (Schneider et al., 2012).

Journal of Cell Science (2022) 135, jcs259893. doi:10.1242/jcs.259893

Electron microscopy thin section

The non-induced and induced TFK1 RNAi knockdown BSF cell pellets were placed on the surface of a copper EM grid (400 mesh) that had been coated with formvar. Each grid was very quickly submersed in liquid propane precooled and held at −180°C by liquid nitrogen as described in Blancard and Salin (2017). Briefly, the loops were then transferred in a pre-cooled solution of 4% osmium tetroxide in dry acetone in a 1.8 ml polypropylene vial at −84°C for 72 h (substitution), warmed gradually to room temperature (1 h −30°C, 2 h −15°C, 2 h 4°C and 30 min room temperature) followed by three washes in dry acetone. The samples were infiltrated progressively with araldite (epoxy resin Fluka). Ultrathin sections were contrasted with lead citrate and observed at 80 kV on a Hitachi 7650 transmission electron microscope.

Immunoelectron microscopy

500 ml of mid-log phase procyclic SmOxP427 cell line expressing endogenously tagged TFK1::3HA were harvested at 1000 ***g***, for 5 min, washed twice with PBS by centrifugation (1000 ***g*** for 5 min) and resuspended in PBS. Freshly glow-discharged, formvar and carbon-coated G2000-ni nickel grids (EMS) were floated on a droplet of cells for 15 min. Grids were then moved onto a drop of 1% NP-40 in PEME buffer (100 mM PIPES pH 6.8, 1 mM $MgCl_2$, 0.1 mM EGTA) 5 min at RT to extract the cells. Cytoskeletons were washed twice (2×5 min) in PEME buffer at RT, equilibrated and blocked on 50 µl drops of 2% fish skin gelatin (Sigma-Aldrich G7041) or blocking buffer (0.5% BSA, 0.1% Tween 20 in PBS), then incubated on 25 µl of primary antibody diluted in blocking buffer (primary antibody was used either alone, or mixed with a second primary antibody) for 1 h at room temperature (RT). Mouse IgG1 anti-TFK1 purified monoclonal antibody was diluted 1:500. Grids were blocked and incubated in secondary antibody for 1 h at RT (goat anti-mouse GMTA 5 nm gold, BBInternational) 1:10 in 0.2% fish skin gelatin in PBS. Grids were blocked and fixed in 2.5% glutaraldehyde in 0.2% fish skin gelatin in PBS. Samples were negatively stained with 1% aurothioglucose (Sigma-Aldrich) (10 µl for 30 s), Micrographs were taken on a Philips Tecnai 12 transmission electron microscope at 100 kV.

Ultrastructure expansion microscopy

The protocol used to perform U-ExM on trypanosomes has been described, adapted and optimized from Gambarotto et al. (2021) and is described in the online protocol at https://doi.org/10.17504/protocols.io.bvwqn7dw. Briefly, 4×10^6 cells of the mid-log phase procyclic SmOx cell line expressing endogenously tagged TFK1::3HA, mNeonGreen::CEP164C or both 10TY1::TbRP2 plus TFK1::3HA were loaded onto poly-L-lysine 0.1% solution (Sigma-Aldrich, P8920)-coated 12 mm coverslips in 24-well plates and cells left to adhere for 5–10 min. Cells were covered with 1 ml of activation solution (0.7% formaldehyde, 1% Acrylamide in PBS) for 4 h at 37°C with slow agitation. For the gelation step, coverslips were gently deposited on top of a 35 µl drop of MS solution [23% sodium acrylate (AK scientific R624), 10% acrylamide (Euromedex EU0060-A), 0.1% bis-acrylamide (Euromedex EU0560-A) in PBS] for 2 min then transferred to a 35 µl drop of MS solution with 0.5% TEMED (Euromedex 50406-A) and 0.5% ammonium persulfate (Euromedex EU0009-A) for 5 min on ice then transferred at 37°C and incubated for 1 h in a moist chamber without agitation. The coverslips were then transferred to a 6-well plate in 1 ml of denaturation solution (200 mM SDS, 200 mM sodium chloride, 50 mM Tris-HCl pH 9.0) with agitation at RT for 15 min to detach the gel from the coverslip, that was then moved into a 1.5 ml Eppendorf centrifuge tube filled with denaturation solution and incubated at 95°C for one 90 min. Gels were expanded in large volumes of deionized water (twice 30 min then overnight) then incubated in a large volume of PBS for 10 min (three times). Small pieces of the gels were processed for immunolabelling as follows. The gels were preincubated in blocking solution (PBS, 2% BSA and 0.2% Tween20) for 30 min at 37°C, and then with primary antibodies [rabbit polyclonal anti-BLD10 (Dang et al., 2017), 1:500 dilution; rabbit polyclonal anti-BILBO1, dilution 1:1000 (Florimond et al., 2015); monoclonal mouse IgG1 anti-HA, 1:500 dilution (Biolegend, 901513); anti-HA (mouse monoclonal IgG2a, Genetex, GTX628902, 1:200); rabbit polyclonal anti-mNeonGreen (Ximbio, 155278), 1:1000 dilution] diluted in blocking solution for 3 h in the dark at 37°C with slow agitation. After three washes in blocking solution, gels were incubated with the secondary antibodies (anti-rabbit-IgG Alexa Fluor 594-conjugated 1:500 dilution (Molecular Probes, goat, A11012); anti-mouse-IgG Alexa Fluor 488-conjugated, 1:500 dilution (Molecular Probes, O-6380); anti-mouse-IgG1-specific Alexa Fluor 594 conjugated, 1:500 dilution (Molecular Probes, A21125); anti-mouse-IgG2a-specific Alexa Fluor 488-conjugated, 1:500 dilution (Molecular Probes, A21131) diluted in blocking solution for 3 h in the dark at 37°C with slow agitation. After three washes in blocking solution, gels were expanded in a large volume of deionized water (twice 30 min then overnight). An expansion factor was determined using the ratio between the size of the coverslip (12 mm) and the size of the gels after the first expansion. U-ExM images were acquired on a Zeiss Imager Z1 microscope with Zeiss 63× oil objectives (NA 1.4), using a Photometrics Coolsnap HQ2 camera and Metamorph software (Molecular Devices) and processed with ImageJ (Schneider et al., 2012).

Scanning electron microscopy

BSF WT and BSF TFK1 24 h RNAi knockdown cell expressing endogenously tagged 10TY1::TFK1 were washed in vPBS and loaded onto 12 mm coverslips coated with poly-L-lysine 0.1% solution (Sigma-Aldrich, P8920) for 30 min. Samples were then fixed with glutaraldehyde (2.5%) in 0.1 M cacodylate buffer (pH 7.2) for 30 min at RT then overnight at 4°C. They were further washed twice in 0.1 M cacodylate buffer and dehydrated in a series of increasing ethanol concentrations (30–100%). Samples were dried via critical point drying (Leica EM CPD300, Austria). Afterwards, the coverslips were mounted onto stubs and coated with platinum, using a sputter coater (Q150T, Quorum Technologies, Kent, UK). Observations and images acquisitions were done at 3.5 kV, in ‘high vacuum’ mode, using a GeminiSEM 300 FESEM (ZEISS Germany) and processed with ImageJ software.

Yeast two-hybrid assay

The pGAD-T7 vectors were transformed in the appropriate yeast haploid cell line Y187 and the pGBK-T7 were transformed in the Y2HGold yeast haploid cell line. After production of diploid cells by yeast mating, interaction tests were carried out on SC –L –W –Histidine (His) medium using drop test assay as described in the online protocol at https://dx.doi.org/10.17504/protocols.io.btzenp3e (Isch et al., 2021).

Protein purification

The *E. coli* BL21 (DE3) (Novagen) bacterial strain was transformed by heat-shock method with pET28a+-TFK1-6His and grown in 200 ml of lysogeny broth (LB) plus kanamycin 50 mg/ml at 37°C and 250 rpm. When an optical density at 600 nm (OD_{600}) of ∼0.6 was reached, cells were then subjected to cold shock on ice for 30 min. Protein expression of recombinant TFK1::6His was induced by adding 1 mM of isopropyl-β-D-thiogalactopyranoside for 3 h at 37°C overnight and 250 rpm. Cells were harvested by centrifugation (16,000 ***g*** for 5 min) and then resuspended in the lysis buffer containing 20 mM Tris-HCl, pH 7.4, 0.5 M NaCl, 20 mM imidazole and 10% (v/v) glycerol, protease inhibitor cocktail (Set III Calbiochem; Ref. 539134-1 at 1:10,000 dilution). Cells were lysed by sonication and cell debris were pelleted by centrifugation (40,000 ***g***, 30 min, 4°C). The supernatant was filtered (0.45-µm pore size, Amicon) and loaded onto a 1 ml HisTrapTMFF column (GE Healthcare) which was pre-equilibrated with the same lysis buffer. The column was washed with five column volumes (CVs) of lysis running buffer and bound protein was eluted with 500 mM imidazole in running buffer with 10 CVs. Elutions containing the highest concentration of purified recombinant TFK1::6His were run on a 10% SDS-PAGE gel then stained with Coomassie Brilliant Blue (Instant Blue^{TM} Expedeon Ltd). Purified recombinant TFK1::6His from a second identically loaded gel was transferred to a PVDF membrane using a semi-dry transfer method (Bio-Rad) and a western blot was performed using anti-His antibody (Sigma H-1029, mouse, 1:3000) to detect the His tag, followed by anti-mouse-IgG HRP-conjugated (Jackson, 115-035-044, 1:10,000).

Monoclonal antibody production

Monoclonal antibodies were raised against purified TFK1::6His in 3 BALB/c mice using the protocol previously described (Willcox et al., 2012). For immunization, 20 µg of recombinant TFK1::6His protein was emulsified with complete Freund's adjuvant and injected into each footpad of the back legs of each mouse. After 12 days, the mice were boosted with 20 µg of recombinant TFK1::6His protein emulsified with incomplete Freund's adjuvant in the same conditions as the first injection. At day 15, after euthanasia of mice, popliteal lymph nodes were collected and B cells were extracted and fused with the myeloma partner P3U1 in PEG 1500 (Roche Diagnostic). Hybridomas were grown up to confluency and screened by indirect ELISA. Nunc Maxisorp flat 96-well plates were coated with 0.5 µg of TFK1 protein in carbonate buffer and saturated with 0.2% gelatin. After PBS washes, 50 µl of hybridoma supernatants were added and incubated 1 h at 37°C. After PBS washes, a secondary antibody HRP-conjugated anti-mouse IgG+IgM diluted 1:5000 (Jackson ImmunoResearch, 115-035-044) was added for 1 h at 37°C. Revelation was done by ABTS-H_2O_2 0.015% and the absorbance was measured at 405 nm, after PBS washes. Hybridomas, which secreted high levels of specific antibody against recombinant TFK1 protein were cloned by limiting dilutions and screened by immunofluorescence assay on endogenously tagged TFK1::3HA procyclic cells. The monoclonal IgG1 mouse antibody named anti-TFK1 was selected for its highly specific signal on immunofluorescence and western blot assays and used as described in this article.

Ethics statement

Animal experiments were performed in the conventional animal facilities of the University of Bordeaux (France) (approval number of B-33-036-917), with the approval of institutional guidelines determined by the local Ethical Committee of the University of Bordeaux and in conformity with the Ministry for Higher Education and Research and the French Committee of Genetic Engineering (approval number 17621-V5-2018112201234223).

Statistics

Experimental data for growth curves and cell count graphs is representative of n=3 independent experiments with values represented as s.e.m. Unpaired two-tailed Student's t-tests were used to determine the statistical significance between values given as P<0.005.

Acknowledgements
We thank Prof. S. Dean (University of Warwick) for the pPOT vectors and trypanosome transfection protocol; Prof. K. Gull (University of Oxford) and Dr P. Bastin (Institut Pasteur) for the BB2 antibody and the hybridoma; Dr M. Rojo., Dr J. Dompierre (IBGC, Bordeaux) and Dr E. Bertiaux (University of Geneva) for expansion microscopy protocols; Dr L. Zyin (University of Texas) for the anti-TbBLD10 antibody; Dr J. Sunter (Oxford Brookes University) for the L3B2 antibody; Prof. K. Ersfeld (University of Bayreuth) for the 9E10 antibody; Dr F. Bringaud (Université de Bordeaux) for the anti-enolase and anti-FTZC antibodies; Dr N. Biteau (Université de Bordeaux) for the anti-TbPFR2 antibody; and Prof. S. Vaughan (Oxford Brookes University) and Dr P. Bastin (Institut Pasteur) for generous donation of endogenously tagged mNeonGreen::CEP164C and RNAi cell lines.

Competing interests
The authors declare no competing or financial interests.

Author contributions
Conceptualization: M.B., D.R.R., D.D.; Methodology: M.R.R., N.L., E.C., B.S., C.B., M.B., D.R.R., D.D.; Validation: M.B., D.R.R., D.D.; Formal analysis: M.R.R., M.B., D.R.R., D.D.; Investigation: M.B., D.R.R., D.D.; Resources: M.B., D.R.R., D.D.; Writing - original draft: M.R.R., M.B., D.R.R., D.D.; Writing - review & editing: M.R.R., M.B., D.R.R., D.D.; Supervision: D.D.; Project administration: M.B., D.R.R., D.D.; Funding acquisition: M.B., D.R.R.

Funding
This work was funded by the Centre National de la Recherche Scientifique, the Université de Bordeaux, the Agence Nationale de la Recherche (ANR)-FWF PRCI [ANR-20-CE91-0003] to M.B., the LabEx ParaFrap [ANR-11-LABX-0024] to D.R.R., the Fondation pour la Recherche Médicale [FRM FDT202001010783] to M.R.R. and the Ministry of Higher Education, Research and Innovation.

Peer review history
The peer review history is available online at https://journals.biologists.com/jcs/article-lookup/doi/10.1242/jcs.259893.

References

Absalon, S., Kohl, L., Branche, C., Blisnick, T., Toutirais, G., Rusconi, F., Cosson, J., Bonhivers, M., Robinson, D. and Bastin, P. (2007). Basal body positioning is controlled by flagellum formation in Trypanosoma brucei. *PLoS ONE* **2**, e437. doi:10.1371/journal.pone.0000437

Albisetti, A., Florimond, C., Landrein, N., Vidilaseris, K., Eggenspieler, M., Lesigang, J., Dong, G., Robinson, D. R. and Bonhivers, M. (2017). Interaction between the flagellar pocket collar and the hook complex via a novel microtubule-binding protein in Trypanosoma brucei. *PLoS Pathog.* **13**, e1006710. doi:10.1371/journal.ppat.1006710

Altschul, S. (1997). Gapped BLAST and PSI-BLAST: a new generation of protein database search programs. *Nucleic Acids Res.* **25**, 3389-3402. doi:10.1093/nar/25.17.3389

Altschul, S. F., Wootton, J. C., Gertz, E. M., Agarwala, R., Morgulis, A., Schaffer, A. A. and Yu, Y.-K. (2005). Protein database searches using compositionally adjusted substitution matrices. *FEBS J.* **272**, 5101-5109. doi:10.1111/j.1742-4658.2005.04945.x

Amodeo, S., Kalichava, A., Fradera-Sola, A., Bertiaux-Lequoy, E., Guichard, P., Butter, F. and Ochsenreiter, T. (2021). Characterization of the novel mitochondrial genome segregation factor TAP110 in Trypanosoma brucei. *J. Cell Sci.* **134**, jcs254300. doi:10.1242/jcs.254300

Andre, J., Kerry, L., Qi, X., Hawkins, E., Drižytė, K., Ginger, M. L. and McKean, P. G. (2014). An alternative model for the role of RP2 protein in flagellum assembly in the African trypanosome. *J. Biol. Chem.* **289**, 464-475. doi:10.1074/jbc.M113.509521

Atkins, M., Týč, J., Shafiq, S., Ahmed, M., Bertiaux, E., De Castro Neto, A. L., Sunter, J., Bastin, P., Dean, S. D. and Vaughan, S. (2021). CEP164C regulates flagellum length in stable flagella. *J. Cell Biol.* **220**, e202001160. doi:10.1083/jcb.202001160

Auty, H., Torr, S. J., Michoel, T., Jayaraman, S. and Morrison, L. J. (2015). Cattle trypanosomosis: the diversity of trypanosomes and implications for disease epidemiology and control. *Rev. Sci. Tech. OIE* **34**, 587-598. doi:10.20506/rst.34.2.2382

Barbar, E. and Nyarko, A. (2015). Polybivalency and disordered proteins in ordering macromolecular assemblies. *Semin. Cell Dev. Biol.* **37**, 20-25. doi:10.1016/j.semcdb.2014.09.016

Bastin, P., Bagherzadeh, Z., Matthews, K. R. and Gull, K. (1996). A novel epitope tag system to study protein targeting and organelle biogenesis in Trypanosoma brucei. *Mol. Biochem. Parasitol.* **77**, 235-239. doi:10.1016/0166-6851(96)02598-4

Benz, C., Clucas, C., Mottram, J. C. and Hammarton, T. C. (2012). Cytokinesis in Bloodstream Stage Trypanosoma brucei Requires a Family of Katanins and Spastin. *PLoS ONE* **7**, e30367. doi:10.1371/journal.pone.0030367

Bertiaux, E., Mallet, A., Fort, C., Blisnick, T., Bonnefoy, S., Jung, J., Lemos, M., Marco, S., Vaughan, S., Trépout, S. et al. (2018). Bidirectional intraflagellar transport is restricted to two sets of microtubule doublets in the trypanosome flagellum. *J. Cell Biol.* **217**, 4284-4297. doi:10.1083/jcb.201805030

Blancard, C. and Salin, B. (2017). Plunge freezing: a tool for the ultrastructural and immunolocalization studies of suspension cells in transmission electron microscopy. *J. Vis. Exp.* **123**, e54874. doi:10.3791/54874

Blum, M., Chang, H.-Y., Chuguransky, S., Grego, T., Kandasaamy, S., Mitchell, A., Nuka, G., Paysan-Lafosse, T., Qureshi, M., Raj, S. et al. (2021). The InterPro protein families and domains database: 20 years on. *Nucleic Acids Res.* **49**, D344-D354. doi:10.1093/nar/gkaa977

Bonhivers, M., Nowacki, S., Landrein, N. and Robinson, D. R. (2008). Biogenesis of the trypanosome endo-exocytotic organelle is cytoskeleton mediated. *PLoS Biol.* **6**, e105. doi:10.1371/journal.pbio.0060105

Bowler, M., Kong, D., Sun, S., Nanjundappa, R., Evans, L., Farmer, V., Holland, A., Mahjoub, M. R., Sui, H. and Loncarek, J. (2019). High-resolution characterization of centriole distal appendage morphology and dynamics by correlative STORM and electron microscopy. *Nat. Commun.* **10**, 993. doi:10.1038/s41467-018-08216-4

Bringaud, F., Robinson, D. R., Barradeau, S., Biteau, N., Baltz, D. and Baltz, T. (2000). Characterization and disruption of a new Trypanosoma brucei repetitive flagellum protein, using double-stranded RNA inhibition. *Mol. Biochem. Parasitol.* **111**, 283-297. doi:10.1016/S0166-6851(00)00319-4

Broadhead, R., Dawe, H. R., Farr, H., Griffiths, S., Hart, S. R., Portman, N., Shaw, M. K., Ginger, M. L., Gaskell, S. J., McKean, P. G. et al. (2006). Flagellar motility is required for the viability of the bloodstream trypanosome. *Nature* **440**, 224-227. doi:10.1038/nature04541

Broster Reix, C. E., Ramanantsalama, M. R., Di Primo, C., Minder, L., Bonhivers, M., Dacheux, D. and Robinson, D. R. (2021a). Intrabody-induced

cell death by targeting the T. brucei cytoskeletal protein *Tb* BILBO1. *Microbiol. Spectr.* **9**, e00915-21. doi:10.1128/Spectrum.00915-21

Broster Reix, C. E., Florimond, C., Cayrel, A., Mailhé, A., Agnero-Rigot, C., Landrein, N., Dacheux, D., Havlicek, K., Bonhivers, M., Morriswood, B. et al. (2021b). Bhalin, an essential cytoskeleton-associated protein of Trypanosoma brucei linking TbBILBO1 of the flagellar pocket collar with the hook complex. *Microorganisms* **9**, 2334. doi:10.3390/microorganisms9112334

Büscher, P., Cecchi, G., Jamonneau, V. and Priotto, G. (2017). Human African trypanosomiasis. *The Lancet* **390**, 2397-2409. doi:10.1016/S0140-6736(17)31510-6

Carvalho-Santos, Z., Machado, P., Branco, P., Tavares-Cadete, F., Rodrigues-Martins, A., Pereira-Leal, J. B. and Bettencourt-Dias, M. (2010). Stepwise evolution of the centriole-assembly pathway. *J. Cell Sci.* **123**, 1414-1426. doi:10.1242/jcs.064931

Carvalho-Santos, Z., Machado, P., Alvarez-Martins, I., Gouveia, S. M., Jana, S. C., Duarte, P., Amado, T., Branco, P., Freitas, M. C., Silva, S. T. N. et al. (2012). BLD10/CEP135 is a microtubule-associated protein that controls the formation of the flagellum central microtubule pair. *Dev. Cell* **23**, 412-424. doi:10.1016/j.devcel.2012.06.001

Chong, W. M., Wang, W.-J., Lo, C.-H., Chiu, T.-Y., Chang, T.-J., Liu, Y.-P., Tanos, B., Mazo, G., Tsou, M.-F. B., Jane, W.-N. et al. (2020). Super-resolution microscopy reveals coupling between mammalian centriole subdistal appendages and distal appendages. *eLife* **9**, e53580. doi:10.7554/eLife.53580

Dacheux, D., Landrein, N., Thonnus, M., Gilbert, G., Sahin, A., Wodrich, H., Robinson, D. R. and Bonhivers, M. (2012). A MAP6-related protein is present in protozoa and is involved in flagellum motility. *PLoS ONE* **7**, e31344. doi:10.1371/journal.pone.0031344

Dang, H. Q., Zhou, Q., Rowlett, V. W., Hu, H., Lee, K. J., Margolin, W. and Li, Z. (2017). Proximity interactions among basal body components in Trypanosoma brucei identify novel regulators of basal body biogenesis and inheritance. *mBio* **8**, e02120-16. doi:10.1128/mBio.02120-16

Davidge, J. A., Chambers, E., Dickinson, H. A., Towers, K., Ginger, M. L., McKean, P. G. and Gull, K. (2006). Trypanosome IFT mutants provide insight into the motor location for mobility of the flagella connector and flagellar membrane formation. *J. Cell Sci.* **119**, 3935-3943. doi:10.1242/jcs.03203

Dean, S., Sunter, J., Wheeler, R. J., Hodkinson, I., Gluenz, E. and Gull, K. (2015). A toolkit enabling efficient, scalable and reproducible gene tagging in trypanosomatids. *Open Biol.* **5**, 140197. doi:10.1098/rsob.140197

Dean, S., Moreira-Leite, F., Varga, V. and Gull, K. (2016). Cilium transition zone proteome reveals compartmentalization and differential dynamics of ciliopathy complexes. *Proc. Natl. Acad. Sci. USA* **113**, E5135-E5143. doi:10.1073/pnas.1604258113

Dean, S., Sunter, J. D. and Wheeler, R. J. (2017). TrypTag.org: a trypanosome genome-wide protein localisation resource. *Trends Parasitol.* **33**, 80-82. doi:10.1016/j.pt.2016.10.009

Farr, H. and Gull, K. (2012). Cytokinesis in trypanosomes. *Cytoskeleton* **69**, 931-941. doi:10.1002/cm.21074

Field, M. C. and Carrington, M. (2009). The trypanosome flagellar pocket. *Nat. Rev. Microbiol.* **7**, 775-786. doi:10.1038/nrmicro2221

Finn, R. D., Clements, J. and Eddy, S. R. (2011). HMMER web server: interactive sequence similarity searching. *Nucleic Acids Res.* **39**, W29-W37. doi:10.1093/nar/gkr367

Florimond, C., Sahin, A., Vidilaseris, K., Dong, G., Landrein, N., Dacheux, D., Albisetti, A., Byard, E. H., Bonhivers, M. and Robinson, D. R. (2015). BILBO1 is a scaffold protein of the flagellar pocket collar in the pathogen Trypanosoma brucei. *PLoS Pathog.* **11**, e1004654. doi:10.1371/journal.ppat.1004654

Gambarotto, D., Hamel, V. and Guichard, P. (2021). Ultrastructure expansion microscopy (U-ExM). *Methods Cell Biol.* **161**, 57-81. doi:10.1016/bs.mcb.2020.05.006

Garcia-Gonzalo, F. R. and Reiter, J. F. (2017). Open Sesame: how transition fibers and the transition zone control ciliary composition. *Cold Spring Harb. Perspect. Biol.* **9**, a028134. doi:10.1101/cshperspect.a028134

Geimer, S. and Melkonian, M. (2004). The ultrastructure of the *Chlamydomonas reinhardtii* basal apparatus: identification of an early marker of radial asymmetry inherent in the basal body. *J. Cell Sci.* **117**, 2663-2674. doi:10.1242/jcs.01120

Gheiratmand, L., Brasseur, A., Zhou, Q. and He, C. Y. (2013). Biochemical characterization of the bi-lobe reveals a continuous structural network linking the bi-lobe to other single-copied organelles in *Trypanosoma brucei*. *J. Biol. Chem.* **288**, 3489-3499. doi:10.1074/jbc.M112.417428

Gonçalves, J. and Pelletier, L. (2017). The ciliary transition zone: finding the pieces and assembling the gate. *Mol. Cells* **40**, 243-253. doi:10.14348/molcells.2017.0054

Gorilak, P., Pružincová, M., Vachova, H., Olšinová, M., Schmidt Cernohorska, M. and Varga, V. (2021). Expansion microscopy facilitates quantitative super-resolution studies of cytoskeletal structures in kinetoplastid parasites. *Open Biol.* **11**, 210131. doi:10.1098/rsob.210131

Graser, S., Stierhof, Y.-D., Lavoie, S. B., Gassner, O. S., Lamla, S., Le Clech, M. and Nigg, E. A. (2007). Cep164, a novel centriole appendage protein required for primary cilium formation. *J. Cell Biol.* **179**, 321-330. doi:10.1083/jcb.200707181

Greenan, G. A., Vale, R. D. and Agard, D. A. (2020). Electron cryotomography of intact motile cilia defines the basal body to axoneme transition. *J. Cell Biol.* **219**, e201907060. doi:10.1083/jcb.201907060

Gull, K. (1999). The cytoskeleton of trypanosomatid parasites. *Annu. Rev. Microbiol.* **53**, 629-655. doi:10.1146/annurev.micro.53.1.629

Hall, N. A. and Hehnly, H. (2021). A centriole's subdistal appendages: contributions to cell division, ciliogenesis and differentiation. *Open Biol.* **11**, 200399. doi:10.1098/rsob.200399

Hammarton, T. C., Clark, J., Douglas, F., Boshart, M. and Mottram, J. C. (2003). Stage-specific differences in cell cycle control in Trypanosoma brucei revealed by RNA interference of a mitotic cyclin. *J. Biol. Chem.* **278**, 22877-22886. doi:10.1074/jbc.M300813200

Hannaert, V., Albert, M.-A., Rigden, D. J., Theresa da Silva Giotto, M., Thiemann, O., Garratt, R. C., Van Roy, J., Opperdoes, F. R. and Michels, P. A. M. (2003). Kinetic characterization, structure modelling studies and crystallization of Trypanosoma brucei enolase. *Eur. J. Biochem.* **270**, 3205-3213. doi:10.1046/j.1432-1033.2003.03692.x

Harmer, J., Qi, X., Toniolo, G., Patel, A., Shaw, H., Benson, F. E., Ginger, M. L. and McKean, P. G. (2017). Variation in basal body localisation and targeting of trypanosome RP2 and FOR20 proteins. *Protist* **168**, 452-466. doi:10.1016/j.protis.2017.07.002

Hatch, E. and Stearns, T. (2010). The life cycle of centrioles. *Cold Spring Harb. Symp. Quant. Biol.* **75**, 425-431. doi:10.1101/sqb.2010.75.054

Hilton, N. A., Sladewski, T. E., Perry, J. A., Pataki, Z., Sinclair-Davis, A. N., Muniz, R. S., Tran, H. L., Wurster, J. I., Seo, J. and de Graffenried, C. L. (2018). Identification of TOEFAZ1-interacting proteins reveals key regulators of Trypanosoma brucei cytokinesis. *Mol. Microbiol.* **109**, 306-326. doi:10.1111/mmi.13986

Hiraki, M., Nakazawa, Y., Kamiya, R. and Hirono, M. (2007). Bld10p constitutes the cartwheel-spoke tip and stabilizes the 9-fold symmetry of the centriole. *Curr. Biol.* **17**, 1778-1783. doi:10.1016/j.cub.2007.09.021

Hodges, M. E., Scheumann, N., Wickstead, B., Langdale, J. A. and Gull, K. (2010). Reconstructing the evolutionary history of the centriole from protein components. *J. Cell Sci.* **123**, 1407-1413. doi:10.1242/jcs.064873

Hughes, L., Towers, K., Starborg, T., Gull, K. and Vaughan, S. (2013). A cell-body groove housing the new flagellum tip suggests an adaptation of cellular morphogenesis for parasitism in the bloodstream form of Trypanosoma brucei. *J. Cell Sci.* **126**, 5748-5757. doi:10.1242/jcs.139139

Hughes, L., Borrett, S., Towers, K., Starborg, T. and Vaughan, S. (2017). Patterns of organelle ontogeny through a cell cycle revealed by whole-cell reconstructions using 3D electron microscopy. *J. Cell Sci.* **130**, 637-647. doi:10.1242/jcs.198887

Ikeda, K. N. and de Graffenried, C. L. (2012). Polo-like kinase is necessary for flagellum inheritance in *Trypanosoma brucei*. *J. Cell Sci.* **125**, jcs.101162. doi:10.1242/jcs.101162

Inoko, A., Yano, T., Miyamoto, T., Matsuura, S., Kiyono, T., Goshima, N., Inagaki, M. and Hayashi, Y. (2018). Albatross/FBF1 contributes to both centriole duplication and centrosome separation. *Genes Cells* **23**, 1023-1042. doi:10.1111/gtc.12648

Isch, C., Majneri, P., Landrein, N., Pivovarova, Y., Lesigang, J., Lauruol, F., Robinson, D. R., Dong, G. and Bonhivers, M. (2021). Structural and functional studies of the first tripartite protein complex at the Trypanosoma brucei flagellar pocket collar. *PLoS Pathog.* **17**, e1009329. doi:10.1371/journal.ppat.1009329

Jana, S. C., Marteil, G. and Bettencourt-Dias, M. (2014). Mapping molecules to structure: unveiling secrets of centriole and cilia assembly with near-atomic resolution. *Curr. Opin. Cell Biol.* **26**, 96-106. doi:10.1016/j.ceb.2013.12.001

Jonsdottir, A. B., Dirks, R. W., Vrolijk, J., Ögmundsdottir, H. M., Tanke, H. J., Eyfjörd, J. E. and Szuhai, K. (2010). Centriole movements in mammalian epithelial cells during cytokinesis. *BMC Cell Biol.* **11**, 34. doi:10.1186/1471-2121-11-34

Joo, K., Kim, C. G., Lee, M.-S., Moon, H.-Y., Lee, S.-H., Kim, M. J., Kweon, H.-S., Park, W.-Y., Kim, C.-H., Gleeson, J. G. et al. (2013). CCDC41 is required for ciliary vesicle docking to the mother centriole. *Proc. Natl. Acad. Sci. USA* **110**, 5987-5992. doi:10.1073/pnas.1220927110

Katoh, Y., Chiba, S. and Nakayama, K. (2020). Practical method for superresolution imaging of primary cilia and centrioles by expansion microscopy using an amplibody for fluorescence signal amplification. *Mol. Biol. Cell* **31**, 2195-2206. doi:10.1091/mbc.E20-04-0250

Kobayashi, T. and Dynlacht, B. D. (2011). Regulating the transition from centriole to basal body. *J. Cell Biol.* **193**, 435-444. doi:10.1083/jcb.201101005

Kohl, L., Sherwin, T. and Gull, K. (1999). Assembly of the paraflagellar rod and the flagellum attachment zone complex during the Trypanosoma brucei cell cycle. *J. Eukaryot. Microbiol.* **46**, 105-109. doi:10.1111/j.1550-7408.1999.tb04592.x

Kuhn, M., Hyman, A. A. and Beyer, A. (2014). Coiled-coil proteins facilitated the functional expansion of the centrosome. *PLoS Comput. Biol.* **10**, e1003657. doi:10.1371/journal.pcbi.1003657

Kumar, D. and Reiter, J. (2021). How the centriole builds its cilium: of mothers, daughters, and the acquisition of appendages. *Curr. Opin. Struct. Biol.* **66**, 41-48. doi:10.1016/j.sbi.2020.09.006

Kumar, P. and Wang, C. C. (2005). Depletion of anaphase-promoting complex or cyclosome (APC/C) subunit homolog APC1 or CDC27 of Trypanosoma brucei arrests the procyclic form in metaphase but the bloodstream form in anaphase. *J. Biol. Chem.* **280**, 31783-31791. doi:10.1074/jbc.M504326200

Kurasawa, Y., Hu, H., Zhou, Q. and Li, Z. (2018). The trypanosome-specific protein CIF3 cooperates with the CIF1 protein to promote cytokinesis in Trypanosoma brucei. *J. Biol. Chem.* **293**, 10275-10286. doi:10.1074/jbc.RA118.003113

Kurasawa, Y., Lee, K. J. and Li, Z. (2022). Structural domains of CIF3 required for interaction with cytokinesis regulatory proteins and for cytokinesis initiation in Trypanosoma brucei. *mSphere* **7**, e00047-22. doi:10.1128/msphere.00047-22

Lacomble, S., Vaughan, S., Gadelha, C., Morphew, M. K., Shaw, M. K., McIntosh, J. R. and Gull, K. (2009). Three-dimensional cellular architecture of the flagellar pocket and associated cytoskeleton in trypanosomes revealed by electron microscope tomography. *J. Cell Sci.* **122**, 1081-1090. doi:10.1242/jcs.045740

Lacomble, S., Vaughan, S., Gadelha, C., Morphew, M. K., Shaw, M. K., McIntosh, J. R. and Gull, K. (2010). Basal body movements orchestrate membrane organelle division and cell morphogenesis in Trypanosoma brucei. *J. Cell Sci.* **123**, 2884-2891. doi:10.1242/jcs.074161

LaCount, D. J., Barrett, B. and Donelson, J. E. (2002). Trypanosoma brucei FLA1 is required for flagellum attachment and cytokinesis. *J. Biol. Chem.* **277**, 17580-17588. doi:10.1074/jbc.M200873200

Laemmli, U. K. (1970). Cleavage of structural proteins during the assembly of the head of bacteriophage T4. *Nature* **227**, 680-685. doi:10.1038/227680a0

Lai, D.-H., Moreira-Leite, F., Xu, Z.-S., Yang, J. and Gull, K. (2021). A specific basal body linker protein provides the connection function for basal body inheritance in trypanosomes. *Proc. Natl. Acad. Sci. USA* **118**, e2014040118. doi:10.1073/pnas.2014040118

Langousis, G. and Hill, K. L. (2014). Motility and more: the flagellum of Trypanosoma brucei. *Nat. Rev. Microbiol.* **12**, 505-518. doi:10.1038/nrmicro3274

Lemos, M., Mallet, A., Bertiaux, E., Imbert, A., Rotureau, B. and Bastin, P. (2020). Timing and original features of flagellum assembly in trypanosomes during development in the tsetse fly. *Parasit. Vectors* **13**, 169. doi:10.1186/s13071-020-04026-0

Madeira, F., Park, Y. M., Lee, J., Buso, N., Gur, T., Madhusoodanan, N., Basutkar, P., Tivey, A. R. N., Potter, S. C., Finn, R. D. et al. (2019). The EMBL-EBI search and sequence analysis tools APIs in 2019. *Nucleic Acids Res.* **47**, W636-W641. doi:10.1093/nar/gkz268

Matsuura, K., Lefebvre, P. A., Kamiya, R. and Hirono, M. (2004). Bld10p, a novel protein essential for basal body assembly in Chlamydomonas. *J. Cell Biol.* **165**, 663-671. doi:10.1083/jcb.200402022

Matthews, K. R. (1999). Developments in the Differentiation of Trypanosoma brucei. *Parasitol. Today* **15**, 76-80. doi:10.1016/S0169-4758(98)01381-7

McAllaster, M. R., Ikeda, K. N., Lozano-Núñez, A., Anrather, D., Unterwurzacher, V., Gossenreiter, T., Perry, J. A., Crickley, R., Mercadante, C. J., Vaughan, S. et al. (2015). Proteomic identification of novel cytoskeletal proteins associated with TbPLK, an essential regulator of cell morphogenesis in Trypanosoma brucei. *Mol. Biol. Cell* **26**, 3013-3029. doi:10.1091/mbc.E15-04-0219

Melville, S. E., Leech, V., Navarro, M. and Cross, G. A. M. (2000). The molecular karyotype of the megabase chromosomes of Trypanosoma brucei stock 427. *Mol. Biochem. Parasitol.* **111**, 261-273. doi:10.1016/S0166-6851(00)00316-9

Mennella, V., Keszthelyi, B., McDonald, K. L., Chhun, B., Kan, F., Rogers, G. C., Huang, B. and Agard, D. A. (2012). Subdiffraction-resolution fluorescence microscopy reveals a domain of the centrosome critical for pericentriolar material organization. *Nat. Cell Biol.* **14**, 1159-1168. doi:10.1038/ncb2597

Morga, B. and Bastin, P. (2013). Getting to the heart of intraflagellar transport using Trypanosoma and Chlamydomonas models: the strength is in their differences. *Cilia* **2**, 16. doi:10.1186/2046-2530-2-16

Morgan, G. W., Denny, P. W., Vaughan, S., Goulding, D., Jeffries, T. R., Smith, D. F., Gull, K. and Field, M. C. (2005). An evolutionarily conserved coiled-coil protein implicated in polycystic kidney disease is involved in basal body duplication and flagellar biogenesis in *Trypanosoma brucei*. *Mol. Cell. Biol.* **25**, 3774-3783. doi:10.1128/MCB.25.9.3774-3783.2005

Morriswood, B., He, C. Y., Sealey-Cardona, M., Yelinek, J., Pypaert, M. and Warren, G. (2009). The bilobe structure of Trypanosoma brucei contains a MORN-repeat protein. *Mol. Biochem. Parasitol.* **167**, 95-103. doi:10.1016/j.molbiopara.2009.05.001

Nachury, M. V. (2018). The molecular machines that traffic signaling receptors into and out of cilia. *Curr. Opin. Cell Biol.* **51**, 124-131. doi:10.1016/j.ceb.2018.03.004

Nett, I. R. E., Martin, D. M. A., Miranda-Saavedra, D., Lamont, D., Barber, J. D., Mehlert, A. and Ferguson, M. A. J. (2009). The phosphoproteome of bloodstream form *Trypanosoma brucei*, causative agent of African sleeping sickness. *Mol. Cell. Proteomics MCP* **8**, 1527-1538. doi:10.1074/mcp.M800556-MCP200

Ogbadoyi, E. O., Robinson, D. R. and Gull, K. (2003). A high-order *Trans* -membrane structural linkage is responsible for mitochondrial genome positioning and segregation by flagellar basal bodies in trypanosomes. *Mol. Biol. Cell* **14**, 1769-1779. doi:10.1091/mbc.e02-08-0525

O'Toole, E. T., Giddings, T. H., McIntosh, J. R. and Dutcher, S. K. (2003). Three-dimensional organization of basal bodies from wild-type and δ-tubulin deletion strains of *Chlamydomonas reinhardtii*. *Mol. Biol. Cell* **14**, 2999-3012. doi:10.1091/mbc.e02-11-0755

Overath, P. and Engstler, M. (2004). Endocytosis, membrane recycling and sorting of GPI-anchored proteins: Trypanosoma brucei as a model system: The endocytic system of T. brucei. *Mol. Microbiol.* **53**, 735-744. doi:10.1111/j.1365-2958.2004.04224.x

Paintrand, M., Moudjou, M., Delacroix, H. and Bornens, M. (1992). Centrosome organization and centriole architecture: Their sensitivity to divalent cations. *J. Struct. Biol.* **108**, 107-128. doi:10.1016/1047-8477(92)90011-X

Pearson, C. G. (2014). Choosing sides–asymmetric centriole and basal body assembly. *J. Cell Sci.* **127**, 2803-2810. doi:10.1242/jcs.151761

Perdomo, D., Berdance, E., Lallinger-Kube, G., Sahin, A., Dacheux, D., Landrein, N., Cayrel, A., Ersfeld, K., Bonhivers, M., Kohl, L. et al. (2022). TbKINX1B: a novel BILBO1 partner and an essential protein in bloodstream form *Trypanosoma brucei*. *Parasite* **29**, 14. doi:10.1051/parasite/2022015

Piel, M., Nordberg, J., Euteneuer, U. and Bornens, M. (2001). Centrosome-dependent exit of cytokinesis in animal cells. *Science* **291**, 1550-1553. doi:10.1126/science.1057330

Poon, S. K., Peacock, L., Gibson, W., Gull, K. and Kelly, S. (2012). A modular and optimized single marker system for generating Trypanosoma brucei cell lines expressing T7 RNA polymerase and the tetracycline repressor. *Open Biol.* **2**, 110037. doi:10.1098/rsob.110037

Pradel, L. C., Bonhivers, M., Landrein, N. and Robinson, D. R. (2006). NIMA-related kinase *Tb* NRKC is involved in basal body separation in *Trypanosoma brucei*. *J. Cell Sci.* **119**, 1852-1863. doi:10.1242/jcs.02900

Ralston, K. S., Lerner, A. G., Diener, D. R. and Hill, K. L. (2006). Flagellar motility contributes to cytokinesis in Trypanosoma brucei and is modulated by an evolutionarily conserved dynein regulatory system. *Eukaryot. Cell* **5**, 696-711. doi:10.1128/EC.5.4.696-711.2006

Reiter, J. F., Blacque, O. E. and Leroux, M. R. (2012). The base of the cilium: roles for transition fibres and the transition zone in ciliary formation, maintenance and compartmentalization. *EMBO Rep.* **13**, 608-618. doi:10.1038/embor.2012.73

Robinson, D. R., Sherwin, T., Ploubidou, A., Byard, E. H. and Gull, K. (1995). Microtubule polarity and dynamics in the control of organelle positioning, segregation, and cytokinesis in the trypanosome cell cycle. *J. Cell Biol.* **128**, 1163-1172. doi:10.1083/jcb.128.6.1163

Schneider, C. A., Rasband, W. S. and Eliceiri, K. W. (2012). NIH Image to ImageJ: 25 years of image analysis. *Nat. Methods* **9**, 671-675. doi:10.1038/nmeth.2089

Schumann Burkard, G., Jutzi, P. and Roditi, I. (2011). Genome-wide RNAi screens in bloodstream form trypanosomes identify drug transporters. *Mol. Biochem. Parasitol.* **175**, 91-94. doi:10.1016/j.molbiopara.2010.09.002

Sherwin, T., Gull, K. and Vickerman, K. (1989). The cell division cycle of Trypanosoma brucei brucei: timing of event markers and cytoskeletal modulations. *Philos. Trans. R. Soc. Lond. B Biol. Sci.* **323**, 573-588. doi:10.1098/rstb.1989.0037

Sinclair, A. N. and de Graffenried, C. L. (2019). More than microtubules: the structure and function of the subpellicular array in trypanosomatids. *Trends Parasitol.* **35**, 760-777. doi:10.1016/j.pt.2019.07.008

Sinclair-Davis, A. N., McAllaster, M. R. and de Graffenried, C. L. (2017). A functional analysis of TOEFAZ1 uncovers protein domains essential for cytokinesis in *Trypanosoma brucei*. *J. Cell Sci.* **130**, 3918-3932. doi:10.1242/jcs.207209

Slaats, G. G., Ghosh, A. K., Falke, L. L., Le Corre, S., Shaltiel, I. A., van de Hoek, G., Klasson, T. D., Stokman, M. F., Logister, I., Verhaar, M. C. et al. (2014). Nephronophthisis-associated CEP164 regulates cell cycle progression, apoptosis and epithelial-to-mesenchymal transition. *PLoS Genet.* **10**, e1004594. doi:10.1371/journal.pgen.1004594

Stephan, A., Vaughan, S., Shaw, M. K., Gull, K. and McKean, P. G. (2007). An essential quality control mechanism at the eukaryotic basal body prior to intraflagellar transport. *Traffic* **8**, 1323-1330. doi:10.1111/j.1600-0854.2007.00611.x

Steverding, D. (2008). The history of African trypanosomiasis. *Parasit. Vectors* **1**, 3. doi:10.1186/1756-3305-1-3

Sunter, J. D. and Gull, K. (2016). The Flagellum Attachment Zone: 'The Cellular Ruler' of Trypanosome Morphology. *Trends Parasitol.* **32**, 309-324. doi:10.1016/j.pt.2015.12.010

Tanos, B. E., Yang, H.-J., Soni, R., Wang, W.-J., Macaluso, F. P., Asara, J. M. and Tsou, M.-F. B. (2013). Centriole distal appendages promote membrane docking, leading to cilia initiation. *Genes Dev.* **27**, 163-168. doi:10.1101/gad.207043.112

Taylor, A. E. and Godfrey, D. G. (1969). A new organelle of bloodstream salivarian trypanosomes. *J. Protozool.* **16**, 466-470. doi:10.1111/j.1550-7408.1969.tb02302.x

Tischer, J., Carden, S. and Gergely, F. (2021). Accessorizing the centrosome: new insights into centriolar appendages and satellites. *Curr. Opin. Struct. Biol.* **66**, 148-155. doi:10.1016/j.sbi.2020.10.021

Trépout, S., Tassin, A.-M., Marco, S. and Bastin, P. (2018). STEM tomography analysis of the trypanosome transition zone. *J. Struct. Biol.* **202**, 51-60. doi:10.1016/j.jsb.2017.12.005

Journal of Cell Science

Tyler, K. (2001). Anisomorphic cell division by African trypanosomes. *Protist* **152**, 367-378. doi:10.1078/1434-4610-00074

Urbaniak, M. D., Martin, D. M. A. and Ferguson, M. A. J. (2013). Global quantitative SILAC phosphoproteomics reveals differential phosphorylation is widespread between the procyclic and bloodstream form lifecycle stages of *Trypanosoma brucei*. *J. Proteome Res.* **12**, 2233-2244. doi:10.1021/pr400086y

Uversky, V. N. (2013). Under-folded proteins: conformational ensembles and their roles in protein folding, function, and pathogenesis: Under-Folded Proteins. *Biopolymers* **99**, 870-887. doi:10.1002/bip.22298

Uzbekov, R. and Alieva, I. (2018). Who are you, subdistal appendages of centriole? *Open Biol.* **8**, 180062. doi:10.1098/rsob.180062

Varga, V., Moreira-Leite, F., Portman, N. and Gull, K. (2017). Protein diversity in discrete structures at the distal tip of the trypanosome flagellum. *Proc. Natl. Acad. Sci. USA* **114**, E6546-E6555. doi:10.1073/pnas.1703553114

Vaughan, S. and Gull, K. (2016). Basal body structure and cell cycle-dependent biogenesis in Trypanosoma brucei. *Cilia* **5**, 5. doi:10.1186/s13630-016-0023-7

Vickerman, K. (1962). The mechanism of cyclical development in trypanosomes of the Trypanosoma brucei sub-group: An hypothesis based on ultrastructural observations. *Trans. R. Soc. Trop. Med. Hyg.* **56**, 487-495. doi:10.1016/0035-9203(62)90072-X

Wei, Q., Xu, Q., Zhang, Y., Li, Y., Zhang, Q., Hu, Z., Harris, P. C., Torres, V. E., Ling, K. and Hu, J. (2013). Transition fibre protein FBF1 is required for the ciliary entry of assembled intraflagellar transport complexes. *Nat. Commun.* **4**, 2750. doi:10.1038/ncomms3750

Wei, Q., Ling, K. and Hu, J. (2015). The essential roles of transition fibers in the context of cilia. *Curr. Opin. Cell Biol.* **35**, 98-105. doi:10.1016/j.ceb.2015.04.015

Wheeler, R. J., Scheumann, N., Wickstead, B., Gull, K. and Vaughan, S. (2013). Cytokinesis in Trypanosoma brucei differs between bloodstream and tsetse trypomastigote forms: implications for microtubule-based morphogenesis and mutant analysis. *Mol. Microbiol.* **90**, 1339-1355. doi:10.1111/mmi.12436

Wheeler, R. J., Gull, K. and Sunter, J. D. (2019). Coordination of the cell cycle in trypanosomes. *Annu. Rev. Microbiol.* **73**, 133-154. doi:10.1146/annurev-micro-020518-115617

Willcox, C. R., Pitard, V., Netzer, S., Couzi, L., Salim, M., Silberzahn, T., Moreau, J.-F., Hayday, A. C., Willcox, B. E. and Déchanet-Merville, J. (2012). Cytomegalovirus and tumor stress surveillance by binding of a human γδ T cell antigen receptor to endothelial protein C receptor. *Nat. Immunol.* **13**, 872-879. doi:10.1038/ni.2394

Winey, M. and O'Toole, E. (2014). Centriole structure. *Philos. Trans. R. Soc. B Biol. Sci.* **369**, 20130457. doi:10.1098/rstb.2013.0457

Wirtz, E., Leal, S., Ochatt, C. and Cross, G. A. M. (1999). A tightly regulated inducible expression system for conditional gene knock-outs and dominant-negative genetics in Trypanosoma brucei. *Mol. Biochem. Parasitol.* **99**, 89-101. doi:10.1016/S0166-6851(99)00002-X

Woods, A., Sherwin, T., Sasse, R., MacRae, T. H., Baines, A. J. and Gull, K. (1989). Definition of individual components within the cytoskeleton of Trypanosoma brucei by a library of monoclonal antibodies. *J. Cell Sci.* **93**, 491-500. doi:10.1242/jcs.93.3.491

Yang, T. T., Chong, W. M., Wang, W.-J., Mazo, G., Tanos, B., Chen, Z., Tran, T. M. N., Chen, Y.-D., Weng, R. R., Huang, C.-E. et al. (2018). Super-resolution architecture of mammalian centriole distal appendages reveals distinct blade and matrix functional components. *Nat. Commun.* **9**, 2023. doi:10.1038/s41467-018-04469-1

Zhang, X., An, T., Pham, K. T. M., Lun, Z.-R. and Li, Z. (2019). Functional analyses of cytokinesis regulators in bloodstream stage trypanosoma brucei parasites identify functions and regulations specific to the life cycle stage. *mSphere* **4**, e00199-19. doi:10.1128/mSphere.00199-19

Zhou, Q. and Li, Z. (2016). A backup cytokinesis pathway in *Trypanosoma brucei*. *Cell Cycle* **15**, 2379-2380. doi:10.1080/15384101.2016.1181882

Zhou, Q., Gu, J., Lun, Z.-R., Ayala, F. J. and Li, Z. (2016a). Two distinct cytokinesis pathways drive trypanosome cell division initiation from opposite cell ends. *Proc. Natl. Acad. Sci. USA* **113**, 3287-3292. doi:10.1073/pnas.1601596113

Zhou, Q., Hu, H. and Li, Z. (2016b). An EF-hand-containing protein in trypanosoma brucei regulates cytokinesis initiation by maintaining the stability of the cytokinesis initiation factor CIF1. *J. Biol. Chem.* **291**, 14395-14409. doi:10.1074/jbc.M116.726133

Zhou, Q., An, T., Pham, K. T. M., Hu, H. and Li, Z. (2018). The CIF1 protein is a master orchestrator of trypanosome cytokinesis that recruits several cytokinesis regulators to the cytokinesis initiation site. *J. Biol. Chem.* **293**, 16177-16192. doi:10.1074/jbc.RA118.004888